

# The Gordian Knot for VLMs: Diagrammatic Knot Reasoning as a Hard Benchmark

Hao Liu\*

Department of Psychology  
New York University

Jicheng Liu†

Department of Computer Science  
University of Southern California

## Abstract

A vision–language model can look at a knot diagram and report what it sees, yet fail to act on that structure. KNOTBENCH pairs an 858,318-image corpus from 1,951 prime-knot prototypes (crossing numbers 3 to 19) with a protocol whose answers are checked against Regina’s canonical knot signature. Its 14 tasks span four families, equivalence judgment, move prediction, identification, and cross-modal grounding; an image-versus-symbol split locates failures along the perception–operation gap. We score Claude Opus 4.7 and GPT-5, each with and without thinking, under a 64K output-token budget matched on both vendors. Across 56 (task, model) cases, 15 sit at or below a random baseline and 8 of 14 tasks have a best score under  $1.5\times$  random. On diagram-to-symbol transcription, no model produces a strictly correct string, and permissive Regina decoding recovers the knot in 0 to 4 of 100 items. Thinking-mode reasoning lifts overall accuracy by 1.65 points for Claude and 9.25 points for GPT-5, narrowing the gap only modestly. Read together, the four families suggest current vision–language models hold features of a diagram but lack apparatus to simulate moves on those features.

## 1 Introduction

Vision–language models routinely fail on questions that should be easy if seeing meant understanding. They miscount a handful of overlapping circles, mistake which line crosses which, and lose track of containment in simple diagrams [Rahmanzadehgervi et al., 2024, Fu et al., 2024]. A natural reading of these failures is that visual perception is shallow. We think the more telling failure sits one step later. Even when a model’s free-form description correctly names the elements of an image, the same model often cannot act on those elements: it cannot decide whether two such images are equivalent, predict the consequence of a small change, or translate what it just described into a symbolic form that something else can check. This paper studies that second step. We call it the *perception–operation gap*, and we measure it on a domain where the ground truth is mathematical rather than annotated: a model that can perceive a structure but cannot operate on it should be visible as a sharp drop between describing and doing.

Knot diagrams are a clean domain for this measurement. A knot is a closed loop in three dimensions; a knot diagram is its 2D shadow with a small over/under mark at each place two strands cross. The property that matters for us is that the same knot has many diagrams. A trefoil can be drawn with 3, 5, or 20 crossings and the underlying knot is unchanged; the diagrams are

---

\*First author. Correspondence to: h14220@nyu.edu.

†Second author.

related by Reidemeister moves (three local rewrites that change a diagram’s appearance without changing the underlying knot, and whose compositions generate all diagrams of a given knot). Conversely, two diagrams that look almost identical can be topologically distinct. The mutant pair  $K11n34$  and  $K11n42$  (two distinct knots that share the same classical invariants: Jones, Alexander, signature, determinant) is the canonical small example, and an expert needs a careful calculation to tell them apart. Both directions are useful here. Many-drawings-one-knot lets us ask whether a model preserves identity across a deliberately varied visual surface; look-alike-different-knot lets us ask whether it notices a change that matters.

KNOTBENCH turns this into a benchmark. The corpus contains 858,318 PNG renders drawn from 1,951 prime-knot prototypes (a prime knot has at least one crossing and cannot be split into two simpler knots) with reduced crossing number 3 to 19. We generate it by random walks of Reidemeister moves over each prototype; the pipeline is in Section 3. Answers are graded against Regina’s canonical knot signature, a stable string fingerprint that serves as our equivalence oracle. On top of the corpus, the protocol is a 14-task grid organized along two axes: a task family (equivalence judgment A, action prediction B, identification C, cross-modal grounding D) and a modality (-I for image input, -S for PD-code text). The modality axis is what lets us read perception against operation: if a task is solved on its -S variant but not its -I variant, the model can act on the symbolic form yet cannot extract that form from pixels.

Four closed-source models (Claude Opus 4.7 and GPT-5, each with and without thinking-mode reasoning) are scored under a 64K output-token budget matched on both vendors. Across the 56 (task, model) pairs, 15 sit at or below the random baseline and 8 of 14 tasks have a best score under  $1.5\times$  random. No model produces a diagram-to-symbol transcription that decodes to the correct knot; permissive Regina decoding recovers between 0 and 4 knots out of 100. Thinking-mode reasoning lifts overall accuracy by 1.65 points for Claude and 9.25 points for GPT-5, narrowing the gap but not closing it. Across the four task families the four models can see knot diagrams but cannot reliably operate on them: counting, equivalence-checking, transcription, and trajectory reasoning each fail in a different way (Fig. 1).

**Contributions.** (1) The KNOTBENCH corpus, the first dataset of its kind for diagrammatic-knot vision–language reasoning. (2) A 14-task diagnostic protocol with topological ground truth, including mutant-pair hard negatives derived from classical-invariant collisions. (3) Diagnostic findings on four closed-source vision–language models that locate failures to specific operations on perceived structure.

We argue in Section 6 that this pattern is consistent with current models lacking the kind of internal action-simulator that humans recruit for spatial reasoning [Hegarty, 2004].

**Roadmap.** Section 2 introduces knot diagrams. Section 3 describes the corpus. Section 4 defines the 14 tasks. Section 5 reports findings. Section 6 discusses limits and an architectural reading. Section 7 surveys related work.

## 2 Background: knot diagrams

A *knot* is a closed loop of string in 3D, with no loose ends. A *knot diagram* is what you see when you photograph that loop from above: a 2D drawing of the loop on the page, with a small marker at each spot where one strand passes over another to record which strand is on top. Each such over/under spot is a *crossing*. We restrict attention to *prime* knots, the knots that cannot be cut

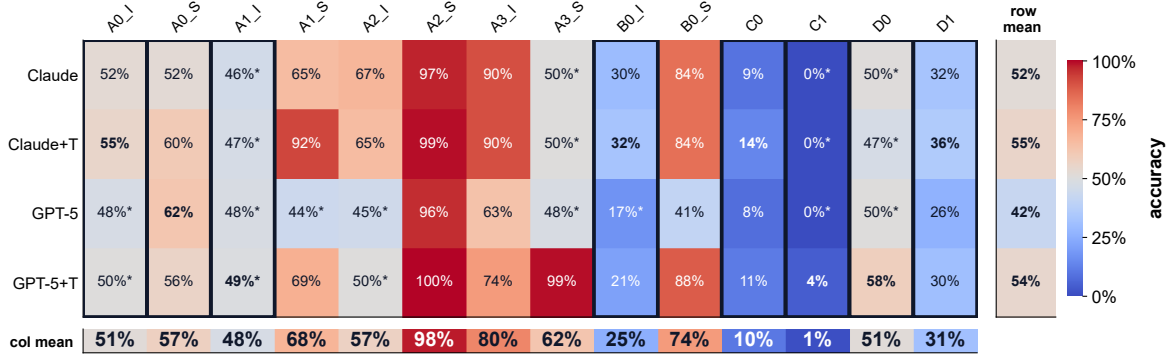


**Figure 1:** At-a-glance summary of the KNOTBENCH results. Rows are the four vision–language models we evaluated; columns are the 14 evaluation tasks; task color is accuracy on a coolwarm scale. The charcoal box marks state-of-the-art accuracy at or below 65%. Most tasks in most rows are well below the white midline, which corresponds to the random baseline for the binary tasks.

into two non-trivial knots tied in series; these are the building blocks of knot theory and the only knots in our corpus.

The same knot admits many different diagrams. Bend the loop in space, photograph it from a different angle, and the crossings move around; the underlying knot is unchanged but the drawing is not. *Reidemeister moves* are the three local edits that capture this freedom: **R1** adds or removes a small kink in a single strand, **R2** adds or removes a bigon where two strands overlap, and **R3** slides one strand across a crossing of the other two. Reidemeister’s theorem [Reidemeister, 1927] states that two diagrams represent the same knot if and only if one can be turned into the other by a finite sequence of R1, R2, and R3 moves. Fig. 2 shows three diagrams of the trefoil produced by such a sequence.

To talk about diagrams precisely we need to write them down. A *PD code* (planar diagram code) lists one 4-tuple per crossing, recording the four arcs that meet there in order around the crossing. The trefoil  $3_1$ , in Regina’s convention, has PD code  $[(1, 4, 2, 5), (3, 6, 4, 1), (5, 2, 6, 3)]$ . A *DT code* (Dowker–Thistlethwaite) is an alphabetical relabelling of the same information optimised for compactness: the same trefoil becomes **bca**. Both fix one diagram; many codes describe the same knot. To check whether two diagrams really do represent the same underlying knot we use Regina’s **knotSig**, a canonical fingerprint of the knot itself [Burton et al., 2024]; two diagrams of the same knot produce identical fingerprints, and two distinct knots produce different ones. We will call this the (*canonical*) *knot signature* throughout the paper. It is not the classical  $\sigma(K)$  signature invariant of knot theory (an integer derived from a Seifert matrix), which we never use as ground truth.

*Mutant pairs* are pairs of distinct knots that agree on most classical invariants. The smallest mutant pair, K11n34 versus K11n42, has identical Jones polynomial, Alexander polynomial, classical signature  $\sigma(K)$ , and determinant, yet the two knots are topologically distinct [Conway, 1970]. Regina’s knot signature separates them; classical invariant collisions do not. We use mutant pairs as hard negatives: a model that scores well on them is not relying on memorised invariants.

For a vision–language model, deciding whether two diagrams depict the same knot decomposes into perception (read each crossing’s over/under structure from pixels) and operation (recognise whether the two diagrams lie in the same Reidemeister equivalence class). Most benchmarks bundle these. KNOTBENCH keeps them apart by varying the input modality between rendered images and PD-code text, which is the structure the next section’s corpus is built to expose.

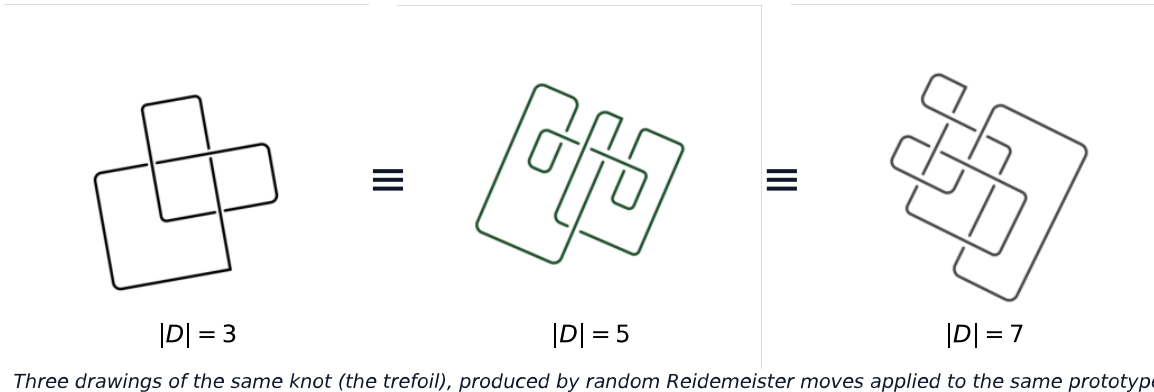


**Figure 2:** Three drawings of the trefoil knot at three different crossing counts, produced by the same prototype under different random sequences of Reidemeister moves. Same knot, different diagram; KNOTBENCH samples broadly from this equivalence class.

**Notation.**

- $K$ : a knot (topological class, identified by its canonical knot signature).
- $D, D'$ : diagrams of  $K$ .
- $|D|$ : crossing count of diagram  $D$ .
- $rc(K)$ : reduced crossing number,  $\min_{D \text{ of } K} |D|$ .
- *Chirality* of a diagram: one of the two mirror-image versions of  $K$ . We fix a chirality choice per prototype; the other is its mirror.

Formal definitions, the mutant theory, amphichiral knots, and the flype move are deferred to Section A.

### 3 The KnotBench corpus

KNOTBENCH contains **858,318** algorithmically generated PNG renders of knot diagrams, drawn from **1,951** prime-knot prototypes spanning reduced crossing number 3 to 19. The size gives each evaluation task hundreds of items per crossing-count tier, the prototype count covers every prime knot Regina tabulates below  $rc = 11$  plus a stratified sample at higher complexity, and the  $rc$  range stretches well past the regime in which a human solves diagrams by inspection. Every render descends from one of the 1,951 prototypes, and Regina’s canonical knot signature on that prototype is the ground truth for the render. Each prototype is rendered many times, on average **440** different ways: chiralities, walk seeds, and textures combine to produce visually distinct diagrams that are nevertheless the same knot. The A-family equivalence tasks (Section 4) lean on this, asking the model to look at two such renders and decide whether they show the same knot.

**How a render is produced.** Figure 3 shows the hierarchy from prototype to leaf: a prototype is paired with both of its chiralities (the diagram and its mirror); for each (prototype, chirality) we run 128 independent random walks; and each walk’s terminal diagram is laid out and rasterized to one PNG. A walk is a Metropolis–Hastings chain whose proposal distribution is the set of Reidemeister moves, with an acceptance rule biased against visually pathological diagrams (self-loops and bigons), and because every move preserves topological identity, every leaf of the tree carries the prototype’s canonical signature exactly. The walk length is sampled uniformly between 80 and 160 steps and the underlying R-move primitives go through Regina [Burton et al., 2024]; the energy function, primitive

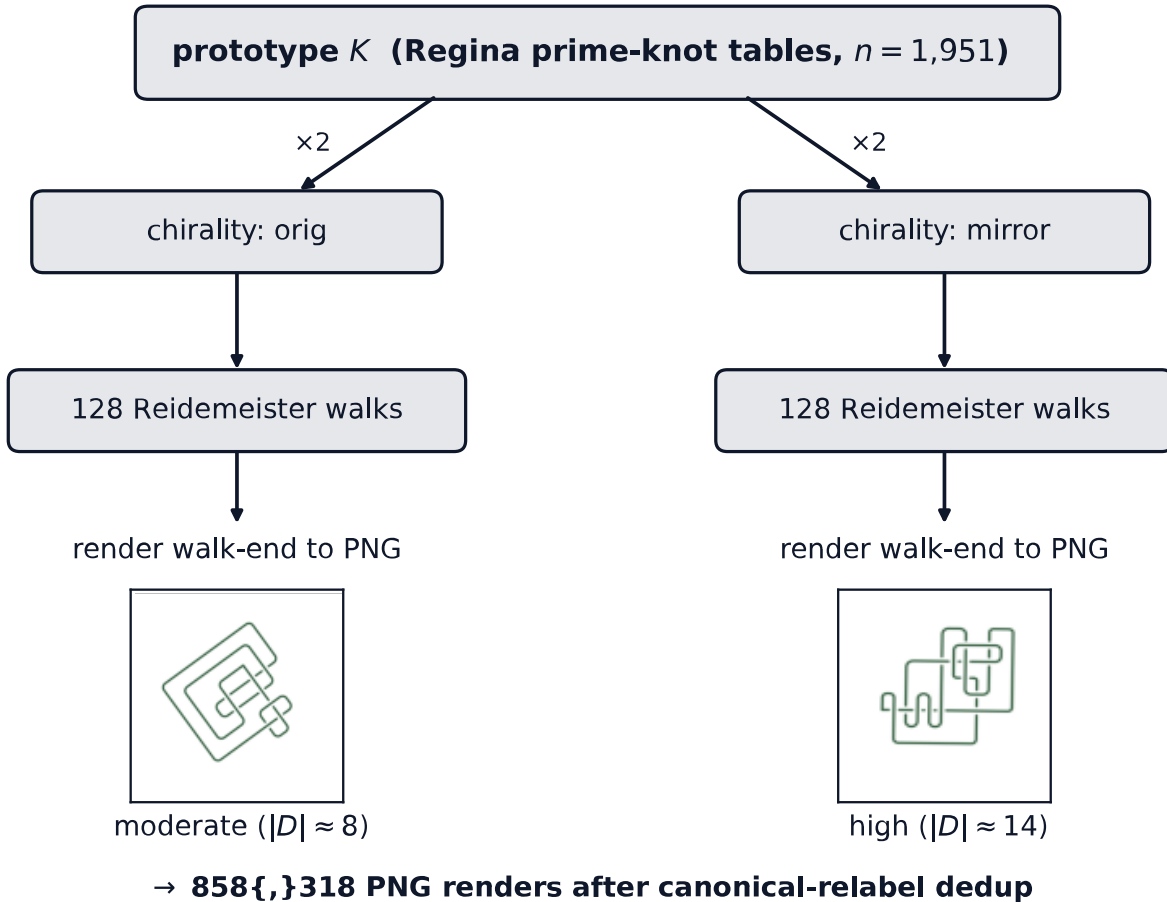


**Figure 3:** Generation tree of the KNOTBENCH corpus. Each prototype is processed at both chiralities; for every (prototype, chirality) we run 128 random walks over Reidemeister moves and render the final diagram. Two example renders are shown at the leaves: a moderate-complexity diagram of a low-rc prototype ( $|D| \approx 8$ ) and a higher-complexity walk-end of a different prototype ( $|D| \approx 14$ ).

table, and lint thresholds are in Section B. In addition to the leaf, every accepted intermediate state is archived, and this trajectory store is the source of items for the B-family move-prediction tasks.

**Coverage along the dimensions a benchmark consumer cares about.** Figure 4 reports the distribution of renders along crossing-count tier, chirality, texture, color rotation, and leaves per prototype. We bin renders into four crossing-count tiers, L1 ( $n_x \in [3, 7]$ ), L2 ( $[8, 13]$ ), L3 ( $[14, 22]$ ), and L3+ ( $[23, 30]$ ); L1 holds only 0.06% of renders because just 14 prime knots have reduced crossing number  $\leq 7$ , a mathematical floor on the prototype side and not a sampling artifact. Chirality and texture are exactly 50/50 by construction, and the seven-color palette and twelve-bin rotation histogram each sit within  $\pm 0.4\%$  of uniform, so visual style introduces no correlated bias. Leaves per prototype average 440, with a cap of 512 set by the  $128 \times 2 \times 2$  product of walks, chiralities, and textures, and the long tail of below-cap prototypes reflects lint rejections rather than topology drift. Across all six dimensions the corpus is the kind of ground for which the equivalence-task design works: many drawings of each knot, drawn diversely, with topology certified.

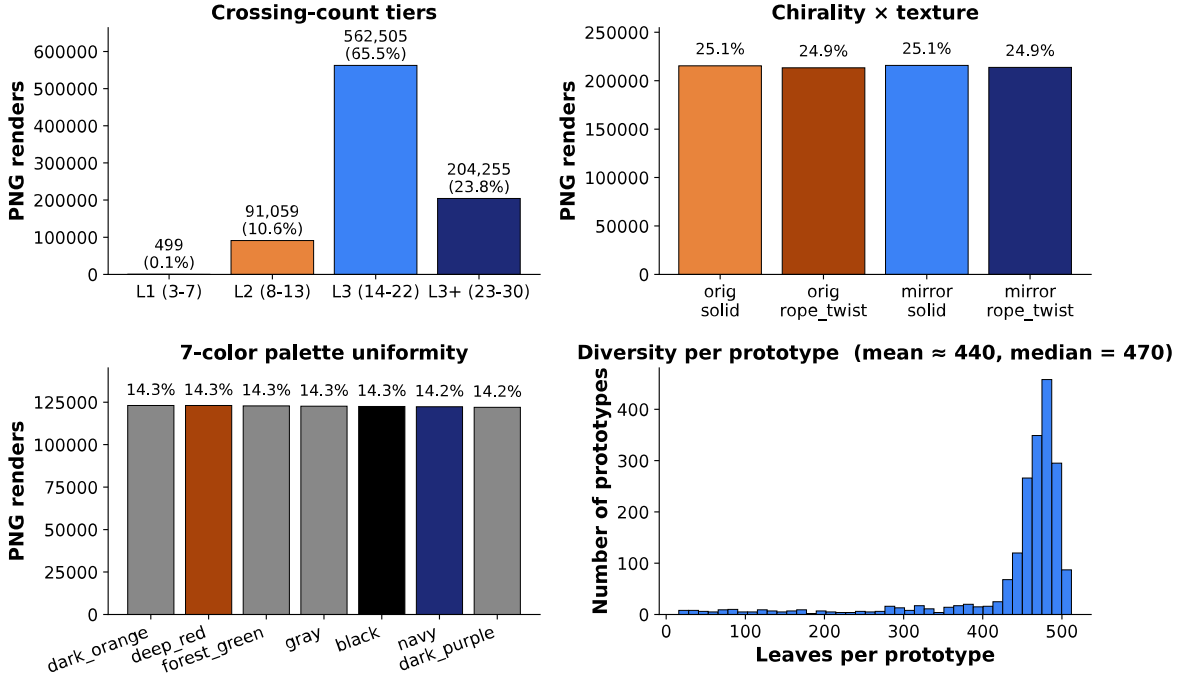


**Figure 4:** Corpus coverage. (Top-left) crossing-count tier breakdown, showing the L1/L2/L3/L3+ split of the 858,318 renders, where tiers are defined by render crossing count  $n_x$ : L1 [3, 7], L2 [8, 13], L3 [14, 22], L3+ [23, 30]. (Top-right) chirality  $\times$  texture combinations, exactly 25% each by construction. (Bottom-left) seven-color palette uniformity (within  $\pm 0.4\%$  of uniform). (Bottom-right) leaves per prototype distribution; mean  $\approx 440$ , cap 512.

**What the corpus is for.** Each render carries the topological identity of its prototype, and the corpus contains many such renders for the same identity. These two facts together are the substrate on which the 14 evaluation tasks of Section 4 test the perception–operation gap. The A-family tasks exploit the many-drawings-of-the-same-knot property to ask whether a model can recognize equivalence under R-moves; mutant pairs (Section 2) serve as the hard negatives that separate recognition-by-features from recognition-by-topology, because a model that decides on classical invariants alone will confuse them. The B-family tasks exploit the trajectory archive to ask whether the model can predict a single move forward. The C- and D-families exploit the symbolic ground truth, the PD code paired with each render, to ask whether a model can cross between visual and symbolic representations.

**Reproducibility.** The corpus is byte-deterministic at the PD-code level: rerunning the pipeline reproduces the manifest’s PD codes exactly. PNG rasterization is byte-stable only when rendering libraries and system fonts are pinned to the versions we used. SHA-256 hashes for the manifest, prototype list, trajectory archive, and rendered PNGs are recorded in the release lockfile; the full seed schedule and version pins are in Section B. With those pins, the corpus and its derived 2,000-item evaluation split are reconstructible from the released artifacts, and we describe how the 14 tasks consume this substrate next.

## 4 The 14-task evaluation

We decompose “visual reasoning over knot diagrams” into 14 tasks grouped into four task families (Fig. 5). Each task asks a single yes/no or short-answer sub-question, scored against topological ground truth. Two axes organise the tasks. The *family* axis (A, B, C, D) varies which operation the model performs on the perceived structure: deciding equivalence, predicting an R-move, identifying a knot, or grounding a symbolic description in pixels. The *modality* axis (-I vs. -S, where applicable) varies whether the diagram arrives as an 800×800 PNG or as PD-code text. When a task is solved on its -S variant but not its -I variant, the model can act on symbolic knot structure but cannot extract that structure from pixels; the cross-modality split is what turns the benchmark into a diagnostic. Table 1 is the 14-row cheat-sheet referenced throughout Section 5.

### 4.1 Task families

**Family A: equivalence ladder.** Four binary same/different judgments at successively finer resolution, each conditioning on the level above. **A0:** same knot, given two arbitrary diagrams (no conditioning). **A1:** same chirality, given the two diagrams are already known to be the same knot. **A2:** same crossing count  $n_x$ , given the two diagrams are the same knot at the same chirality. **A3:** same canonical PD code, given the two diagrams are in the same (proto, chir,  $n_x$ ) bucket. A3 negatives are the visually most similar items in the benchmark (relabellings of strand indices on the same drawing); A0 negatives are the visually most distinct (different knots) and include mutant pairs as hard negatives [Conway, 1970]. Each level has -I and -S variants, giving eight A-tasks in total.

**Family B: action prediction.** **B0:** given two diagrams  $D_t$  and  $D_{t+1}$  from a Reidemeister walk, identify which of  $\{R1^\pm, R2^\pm, R3, \text{NC}\}$  relates them (where NC denotes NOT-CONNECTED). NOT-CONNECTED items are sampled from the trajectory archive as PD pairs at least 5 walk-steps apart; in expectation, a 1-step shortcut between such a pair is a probability-zero event but not strictly impossible (we report the  $\sim 1\%$  residual false-positive risk in Section 6). B0 has -I and -S variants. The task isolates the mental-simulation operation: a solver imagines applying each candidate move to  $D_t$  and checks which result matches  $D_{t+1}$ .

**Family C: identification.** **C0:** given one rendered diagram, output the integer crossing count  $|D|$ . **C1:** given one rendered diagram, transcribe its DT code as a lower-case alphabetical string. For example, the trefoil  $3_1$  has DT code `bca`; a model that outputs `bca` on a trefoil render is correct, whereas `abc` or `baca` are wrong. C0 is scored by exact-match on the integer; C1 is scored both as strict string match and via a permissive Regina-decode pass that checks whether the model’s string, when decoded as a DT code, produces the ground-truth canonical signature. C1 is the cleanest task for the perception-to-symbol direction. C0 and C1 are image-only.

**Family D: cross-modal grounding.** **D0** (binary): given one rendered diagram and one candidate PD code, return whether the code describes the diagram. **D1** (4-way MCQ): given one rendered diagram and four candidate PD codes, select the one that describes it. Both D-tasks are image-grounded, so neither admits a pure-symbolic variant.

## 4.2 Items, models, and scoring

The evaluation set contains 2,000 items, distributed across the 14 tasks as listed in Table 1 and stratified by  $n_x$  bins  $\{8-10, 11-13, 14-16, 17-20\}$ . A0 negatives draw on the corpus’s 39 strict mutant pairs (all four classical invariants match) and 75 Jones-only mutant pairs. The prototype-level split (70.78 / 15.84 / 13.38 % train/val/test) keeps mutant components together so no test pair leaks via invariant collision. The eval set is SHA-256 locked.

We evaluate four vision–language models: Claude Opus 4.7 [Anthropic, 2026] and GPT-5 [OpenAI, 2026], each with and without thinking-mode reasoning enabled. Each task has a fixed prompt template that hides prototype names, uses opaque PNG identifiers, and forces an `ANSWER:` output line (e.g., `ANSWER: yes`, `ANSWER: R3`, `ANSWER: bca`). Strict-match scoring extracts that line and compares against the ground-truth label after case-insensitive normalisation; full templates and parser fallback rules are in Section E. We evaluate under a 64K output-token budget on both vendors.

**Table 1:** The 14 evaluation tasks. “Modality” indicates whether the diagram is delivered as an image (I), as PD-code text (S), or both. Random baselines: 50% for binary yes/no tasks (A0–A3, D0),  $1/6 \approx 16.7\%$  for B0, 25% for D1, and 0% for C0/C1, where exact-match against a free-form output has negligible chance from a uniform guess.

Task	Plain-English question	Modality	$N$	Random
A0-I	Same knot? (two arbitrary diagrams)	I	200	50.0%
A0-S	Same knot? (two PD codes)	S	200	50.0%
A1-I	Same chirality, given same knot? (images)	I	100	50.0%
A1-S	Same chirality, given same knot? (PD codes)	S	100	50.0%
A2-I	Same $n_x$ , given same knot + chirality? (images)	I	100	50.0%
A2-S	Same $n_x$ , given same knot + chirality? (PD codes)	S	100	50.0%
A3-I	Same canonical PD, given same bucket? (images)	I	200	50.0%
A3-S	Same canonical PD, given same bucket? (PD codes)	S	100	50.0%
B0-I	Which R-move connects $D_t$ and $D_{t+1}$ ? (images)	I	200	16.7%
B0-S	Which R-move connects $D_t$ and $D_{t+1}$ ? (PD codes)	S	100	16.7%
C0	How many crossings in this diagram?	I	100	0.0%
C1	What is the DT code of this diagram?	I	100	0.0%
D0	Does this PD code describe this image?	I+S	200	50.0%
D1	Which of these 4 PD codes describes this image?	I+S	200	25.0%

## 5 Results

Table 2 reports top-line accuracy on the 2,000-item evaluation set, and Fig. 1 in Section 1 shows the corresponding  $4 \times 14$  heatmap. We organize the section around five core findings keyed to the perception–operation gap, followed by a short supplementary block and a methodological note on the output-token budget.

### 5.1 Core finding A — models are near random

Of the 56 (task, model) pairs in Table 2, 15 sit at or below the random baseline. Of the 14 tasks, 8 have a state of the art within  $1.5 \times$  random. Fig. 6 plots the per-pair deviation from random, sorted by score.

**Table 2:** Headline accuracy per model on the full 2,000-item evaluation set.

Model	Items	Acc. (%)	Empty
claude-opus-4-7	2,000	51.65	0/2,000
claude-opus-4-7 + thinking	2,000	54.60	4/2,000
gpt-5	2,000	43.00	0/2,000
gpt-5 + thinking	2,000	52.25	19/2,000

Four tasks account for the visible above-random performance. **A2-S** (count crossings given a PD code) sits at  $\geq 96\%$  for all four models; it is a sanity check that the prompt and scoring pipeline are not themselves broken. **A3-I** (same canonical PD given the same bucket) reaches roughly 90% on the two Claude variants, the only image-only task with a model in that range. **B0-S** (predict the R-move connecting two PD codes) is solved by gpt-5+thinking at 88%; we return to this task in finding C, since its image counterpart fails. **A1-S** (same chirality, given same knot, from PD codes) jumps from near random to 80–90% under thinking on both vendors. In every case the symbolic structure is either given as input or is the answer itself; in every other task the model is asked to extract symbolic structure from pixels and then act on it, and the accuracy lands inside the random envelope.

## 5.2 Core finding B — modality matters more than thinking

Both vendors gain from thinking-mode reasoning, but the gain is not distributed evenly across tasks. Aggregate lift is +1.65pt for Claude (51.65  $\rightarrow$  54.60) and +9.25pt for GPT-5 (43.00  $\rightarrow$  52.25), and Fig. 7 shows that almost all of it lands on the symbolic ( $-S$ ) tasks. On A1-S, claude+thinking gains +27pt and gpt-5+thinking gains +25pt; on A3-S, claude+thinking is flat while gpt-5+thinking gains +51pt; on B0-S, claude+thinking is again flat while gpt-5+thinking gains +47pt. Image-only tasks, in contrast, move by single digits or fall.

The within-task A3 contrast makes the asymmetry sharp. A3-I asks whether two rendered diagrams have the same canonical PD code, and A3-S asks the same question about two PD codes directly. Both Claude variants solve A3-I at  $\approx 90\%$  but sit at chance on A3-S, and turning thinking on does not move A3-S. GPT-5 shows the opposite cliff, with A3-S jumping from chance to 51% under thinking and A3-I lifting only from 63% to 75%. The flip direction differs by vendor but the shape is the same: when the symbolic structure is in the prompt, more reasoning tokens convert into more accuracy, and when it has to come out of the pixels, they do not (Fig. 8).

The implication for the perception–operation gap is direct. Each  $-S/-I$  pair holds the operation fixed and varies only how the symbolic structure arrives. When the structure arrives as text, the models can act on it, sometimes near-perfectly. When it has to be recovered from pixels, the same operation collapses. The bottleneck is not the operation; it is the lift from pixels to structure.

## 5.3 Core finding C — B0 is shortcut by always-answer-R3 on GPT-5

GPT-5 without thinking reaches 84% on the R3 items of B0 and stays below 30% on every other class (R1 $^\pm$ , R2 $^\pm$ , NOT-CONNECTED). The marginal answer distribution shows the same pattern: the no-thinking model emits “R3” on a large majority of B0 items regardless of input. Thinking on the symbolic variant removes the shortcut; gpt-5+thinking reaches 88% on B0-S with the per-class balance restored. The image variant does not recover. B0-I stays below 35% across all four models, with no class scoring above random when conditioned on the true label (Fig. 9; see App. B for the per-move confusion breakdown).

B0-I is the action-prediction operation in its purest form. A solver has to perceive two diagrams, hypothesize a candidate R-move, and check whether applying it to  $D_t$  produces  $D_{t+1}$ . On the symbolic variant, where the PD codes are given, GPT-5 can do this once thinking is enabled. On the image variant, where the PD code has to come out of the pixels first, no model solves the task, and the no-thinking GPT-5 substitutes a frequency-prior shortcut for the operation. We use this task as the entry point for the mental-simulation discussion in Section 6.

#### 5.4 Core finding D — crossing counting collapses beyond ten

On C0, the per-model strict-match accuracies are 9% (claude), 14% (claude+thinking), 8% (gpt-5), and 11% (gpt-5+thinking). Conditioning on the ground-truth crossing count  $n_x$ , all four models score near-perfect at  $n_x = 8$  and at chance at  $n_x = 20$ , with a monotone decline in between (Fig. 10; see App. B). The task asks the simplest perceptual operation in the benchmark: report an integer. It collapses outside the low-complexity end of the corpus.

Counting failures in VLMs are known on natural and chart images [Rahmanzadehgervi et al., 2024]. C0 replicates the effect on a domain where “what to count” is unambiguous (each crossing is an explicit ink artifact in the orthogonal render) and where the ground-truth count is exact. The failure is not in deciding what to count, it is in counting it.

#### 5.5 Core finding E — DT-code transcription is unsolvable

On C1, all four models score 0/100 under strict matching. Under the permissive Regina post-pass, which decodes the model’s string as a DT code and checks whether it parses to the correct canonical signature, gpt-5+thinking reaches 4/100 and the other three remain at 0/100. Permissive scoring cannot save the task.

C1 is the perception-to-symbol operation in pure form. The model is given one rendered diagram and asked to produce its DT code, which is the symbolic fingerprint of the very structure shown in the image. Current vision–language models do not produce that fingerprint, with or without thinking, under either scoring rule.

#### 5.6 Supplementary findings

**D0 has a systematic “no” bias.** On D0 (does this PD code describe this image?), all four models default toward “no”. Matching items receive 0–16% “yes” answers; same-task-mismatch items receive 86–100% “no” answers (Fig. 11 in App. B).

**A3-I shows the largest cross-vendor gap.** Among image tasks, A3-I shows the largest spread across models: the Claude variants score  $\approx 90\%$ , gpt-5 scores 63%, and gpt-5+thinking scores 74.5%. Thinking does not close the gap.

**Modality conditions the reasoning lift.** The task-level lift pattern from finding B holds at the model level as well; Fig. 7 indicates that the modality split is the strongest covariate of where reasoning helps.

**At-or-below-random is the typical case.** 8 of 14 tasks have at least one model that sits at or below the random baseline (Fig. 6), including all six image tasks in families B, C, and D.

## 5.7 Output-budget note

All four model runs use a 64K output-token budget, the Claude Opus 4.7 extended-thinking maximum, matched on the OpenAI side so that budget exhaustion is adjudicated identically across vendors. At this cap,  $23/8000 = 0.29\%$  of all (task, model) evaluations emit no visible answer line and are scored as wrong under strict matching. The per-task output-token distribution is in Fig. 18.

## 6 Discussion and limitations

**Limitations.** The full table is in Section H; the main caveats follow. The test split holds 18 unique mutant pairs (the floor for our test ratio over 98 mutant components), reused up to four times across renderings; we report mutant accuracy per-pair and per-rendering. The L1 tier ( $rc \leq 7$ ) holds  $\sim 24$  records and is unstratified across most tasks. “Flype” steps (5% of the walk) are implemented as R3 swaps and should be analysed as additional R3. B0 NOT-CONNECTED carries a  $\sim 1\%$  theoretical false positive from accidental five-step reconnection. The Weisfeiler–Lehman hash is a canonical fingerprint, not a graph-isomorphism invariant; it functions correctly on the canonicalized manifest. Mutant detection uses (Jones, Alexander, signature, determinant) collisions. The A1 amphichiral whitelist is limited to  $rc \leq 10$ . About 0.6% of evaluations hit the 64K extended-thinking ceiling and were scored wrong. The lineup covers two closed-source vendors; Gemini and open-weights baselines are the highest-priority extension.

**Mental simulation as the missing operation.** A human solving B0 typically simulates each candidate Reidemeister move and checks whether the result matches the second diagram [Hegarty, 2004]. Our results suggest that current vision–language models do not have this capability in reliable form: B0-I stays below 35% across all four models, gpt-5 without thinking collapses to an “always R3” shortcut, and within-task A3-I (recognizing two diagrams as the same modulo a crossing relabel) shows large cross-vendor gaps. The pattern is consistent with the cognitive-scientist account that current LLMs lack an internal action-conditioned simulator over perceived state [Lake et al., 2017, Mahowald et al., 2024]. World models with explicit action prediction, of the kind in DreamerV3 [Hafner et al., 2023] or JEPA-style architectures [LeCun, 2022], are the natural class to test against the B0 task. We do not propose an architecture; we propose the benchmark as a target. The recipe (formal ground truth plus transformation-defined equivalence classes) applies to molecular structure, electronic schematics, and similar diagrammatic domains.

**Difficulty for humans.** We do not run a human baseline. The tasks in KNOTBENCH are nevertheless non-trivial for humans: counting crossings on a 17-crossing diagram is tedious; distinguishing two diagrams that differ only by a relabelling of crossings (A3-I) requires care; identifying which Reidemeister move took  $D_t$  to  $D_{t+1}$  requires the mental simulation discussed above; transcribing a diagram into a DT code is something most humans never learn. A model that beats a careful human across KNOTBENCH would have demonstrated capability that meaningfully exceeds human visuospatial routine on perceived structure; current models are not at that bar.

**A note on resources.** This is a two-student project on personal workstations, with no GPU cluster and no shared budget. Corpus generation, evaluation, and analysis cost roughly \$450 in API credits, paid out of pocket. The benchmark therefore carries 100–200 items per task rather than the 1k–10k that a well-resourced effort would. We state this as a fact rather than a request, and

note that the paper documents design and findings; community-funded extensions can scale up the per-task  $N$ , add Gemini and open-weights baselines, and pair the corpus with a human baseline.

## 7 Related work

**VLM perception failures.** A line of recent benchmarks documents that vision–language models fail on perceptual tasks that humans solve trivially: counting, identifying overlap, distinguishing left from right, reading clock hands, and tracking simple geometric relations [Rahmanzadehgervi et al., 2024, Fu et al., 2024, Tong et al., 2024, Chen et al., 2024a, Guan et al., 2024]. Reasoning-oriented multimodal benchmarks (MMMU [Yue et al., 2024], MathVista [Lu et al., 2024], ChartQA [Masry et al., 2022]) document similarly large gaps, but their ground truth is human-annotated and their hard items are selected by heuristic difficulty rather than by structural collision. We differ by carrying formal topological ground truth: the canonical signature decides same/different by Reidemeister equivalence, and hard negatives are mutant pairs that agree on (Jones, Alexander,  $\sigma$ , det) yet are genuinely distinct knots, so distractor difficulty is a property of the invariant lattice rather than of annotator disagreement.

**Diagrammatic reasoning.** The cognitive case for diagrams as a special problem class predates deep learning [Larkin and Simon, 1987, Glasgow et al., 1995]. Subsequent benchmarks include AI2D [Kembhavi et al., 2016] for elementary-school science diagrams, and MolScribe [Qian et al., 2023b] and RxnScribe [Qian et al., 2023a] for chemistry diagrams. These share KNOTBENCH’s concern that diagrams encode symbolic content a model must recover, but their ground truth is empirical (chemists agree on the molecule). We differ by adjudicating with a topological verifier: Reidemeister-equivalence is mathematically defined and computable in milliseconds by Regina, so the labelling process is independent of human reviewers entirely.

**Knots and machine learning.** Most prior work on knots and machine learning operates on *symbolic* features such as PD codes, braid words, and classical invariants, not pixel-level diagrams [Davies et al., 2021, Gukov et al., 2021, Hughes, 2016, Jaretzki, 2023]. Davies et al. predict the signature from braid words, Gukov et al. search for unknotting sequences, and Jaretzki applies geometric deep learning on combinatorial representations. The closest visual analogue is contemporaneous work by Dranowski et al. [2025], who train a supervised CNN to recognise knot type from photographs of physical ropes. We differ by being the first dataset and evaluation suite that tests general-purpose vision–language models on knot *diagrams* at the pixel level under zero-shot prompting, with topological ground truth rather than category labels.

**Reasoning effort and thinking-mode evaluation.** Several recent papers study when chain-of-thought helps a model and when it hurts [Sprague et al., 2024, Liu et al., 2024, Chen et al., 2024b], finding domain-conditioned and overthinking-style regressions, but mostly on text-only tasks where the output-token budget is not a confounder. Cross-vendor comparisons under default settings silently mix reasoning ability with output-budget allocation, because Anthropic’s adaptive thinking and OpenAI’s `reasoning_effort` have very different default budgets (App. C). We differ by exposing this interaction along the I/S modality axis (variable input length, fixed task), and by recommending matching output-token caps across vendors; our own runs use a 64K cap on both.

**Cognitive accounts of operating on perceived structure.** Treisman & Gelade’s feature-integration theory [Treisman and Gelade, 1980] named the ancestor problem of *binding*: attaching

local features to a coherent perceptual object. Lake et al. [2017] and Mahowald et al. [2024] argue, from different angles, that statistical language learners lack the compositional and causal machinery needed to manipulate such objects once perceived; action-conditioned world models [Ha and Schmidhuber, 2018, Hafner et al., 2023, LeCun, 2022] propose an architecture class in which a learned simulator carries the perceived structure through an operation. We differ by being a target rather than a model: a diagnostic benchmark on which any candidate architecture (world models, neuro-symbolic hybrids, or future VLMs) should be testable on the perception-to-operation gap, with the topological verifier providing an external pass/fail signal.

**Hard-negative construction.** KNOTBENCH’s mutant pairs are hard negatives by construction: two distinct knots that agree on  $(\text{Jones}, \text{Alexander}, \sigma, \text{det})$ . The general benefit of hard negatives over random distractors is well known in benchmark hygiene [Chen et al., 2024a, White et al., 2024]. We differ by deriving hard negatives from a structural invariant collision rather than from empirical or heuristic similarity, which gives a falsifiable construction rule and a finite, enumerable pool of candidate pairs.

## 8 Conclusion

KNOTBENCH measures the perception–operation gap on knot diagrams: an 858k-image corpus drawn from 1,951 prime-knot prototypes, scored against Regina’s canonical signature on a 14-task grid that separates seeing a diagram from acting on it. Across four closed-source vision–language models, 15 of 56 tasks sit at or below random, no model transcribes a diagram into a decodable symbolic form, and thinking-mode reasoning narrows the gap without closing it. The pattern is what one expects from systems that recover diagram elements without an internal action-conditioned simulator over them, and benchmarks of this shape are what an architecture built around such a simulator should be evaluated on. Planned extensions add open-weights and Gemini models, paraphrase-invariance tests, a human baseline, and architectures whose central claim is to maintain that simulator.

## References

- Anthropic. Claude Opus 4.7, 2026. Model card.
- Benjamin A. Burton, Ryan Budney, William Pettersson, et al. Regina: Software for low-dimensional topology. <https://regina-normal.github.io/>, 2024.
- Lin Chen, Jinsong Li, Xiaoyi Dong, Pan Zhang, Yuhang Zang, Zehui Chen, Haodong Duan, Jiaqi Wang, Yu Qiao, Dahua Lin, and Feng Zhao. Are we on the right way for evaluating large vision-language models? In *Advances in Neural Information Processing Systems (NeurIPS)*, 2024a.
- Xingyu Chen, Jiahao Xu, Tian Liang, Zhiwei He, Jianhui Pang, Dian Yu, Linfeng Song, Qiuzhi Liu, Mengfei Zhou, Zhuosheng Zhang, Rui Wang, Zhaopeng Tu, Haitao Mi, and Dong Yu. Do NOT think that much for  $2+3=?$  On the overthinking of o1-like LLMs. arXiv:2412.21187, 2024b.
- John H. Conway. An enumeration of knots and links, and some of their algebraic properties. In John Leech, editor, *Computational Problems in Abstract Algebra*, pages 329–358. Pergamon Press, Oxford, 1970.

- Alex Davies, Petar Veličković, Lars Buesing, Sam Blackwell, Daniel Zheng, Nenad Tomašev, Richard Tanburn, Peter Battaglia, Charles Blundell, András Juhász, Marc Lackenby, Geordie Williamson, Demis Hassabis, and Pushmeet Kohli. Advancing mathematics by guiding human intuition with AI. *Nature*, 600(7887):70–74, 2021. doi: 10.1038/s41586-021-04086-x.
- Anne Dranowski, Yura Kabkov, and Daniel Tubbenhauer. On knot detection via picture recognition. arXiv:2510.06284, 2025.
- Xingyu Fu, Yushi Hu, Bangzheng Li, Yu Feng, Haoyu Wang, Xudong Lin, Dan Roth, Noah A. Smith, Wei-Chiu Ma, and Ranjay Krishna. BLINK: Multimodal large language models can see but not perceive. In *Proceedings of the European Conference on Computer Vision (ECCV)*, 2024. doi: 10.1007/978-3-031-73337-6\_9.
- Janice Glasgow, N. Hari Narayanan, and B. Chandrasekaran, editors. *Diagrammatic Reasoning: Cognitive and Computational Perspectives*. AAAI Press / MIT Press, Menlo Park, CA, 1995. ISBN 9780262571128.
- Tianrui Guan, Fuxiao Liu, Xiyang Wu, Ruiqi Xian, Zongxia Li, Xiaoyu Liu, Xijun Wang, Lichang Chen, Furong Huang, Yaser Yacoub, Dinesh Manocha, and Tianyi Zhou. HallusionBench: An advanced diagnostic suite for entangled language hallucination and visual illusion in large vision-language models. In *Proceedings of the IEEE/CVF Conference on Computer Vision and Pattern Recognition (CVPR)*, 2024.
- Sergei Gukov, James Halverson, Fabian Ruehle, and Piotr Sulkowski. Learning to unknot. *Machine Learning: Science and Technology*, 2(2):025035, 2021. doi: 10.1088/2632-2153/abe91f. Preprint: arXiv:2010.16263, 2020.
- David Ha and Jürgen Schmidhuber. World models. arXiv:1803.10122, 2018. Short version: “Recurrent World Models Facilitate Policy Evolution,” NeurIPS 2018.
- Danijar Hafner, Jurgis Pasukonis, Jimmy Ba, and Timothy Lillicrap. Mastering diverse domains through world models. arXiv:2301.04104, 2023.
- Mary Hegarty. Mechanical reasoning by mental simulation. *Trends in Cognitive Sciences*, 8(6): 280–285, 2004. doi: 10.1016/j.tics.2004.04.001.
- Mark C. Hughes. A neural network approach to predicting and computing knot invariants. arXiv:1610.05744, 2016.
- Lennart Jaretzki. Geometric deep learning approach to knot theory. arXiv:2305.16808, 2023.
- Aniruddha Kembhavi, Michael Salvato, Eric Kolve, Minjoon Seo, Hannaneh Hajishirzi, and Ali Farhadi. A diagram is worth a dozen images. In *Proceedings of the European Conference on Computer Vision (ECCV)*, 2016.
- Brenden M. Lake, Tomer D. Ullman, Joshua B. Tenenbaum, and Samuel J. Gershman. Building machines that learn and think like people. *Behavioral and Brain Sciences*, 40:e253, 2017. doi: 10.1017/S0140525X16001837.
- Jill H. Larkin and Herbert A. Simon. Why a diagram is (sometimes) worth ten thousand words, 1987.

- Yann LeCun. A path towards autonomous machine intelligence. OpenReview <https://openreview.net/forum?id=BZ5a1r-kVsf>, 2022. Version 0.9.2.
- Ryan Liu, Jiayi Geng, Addison J. Wu, Ilia Sucholutsky, Tania Lombrozo, and Thomas L. Griffiths. Mind your step (by step): Chain-of-thought can reduce performance on tasks where thinking makes humans worse. arXiv:2410.21333, 2024.
- Pan Lu, Hritik Bansal, Tony Xia, Jiacheng Liu, Chunyuan Li, Hannaneh Hajishirzi, Hao Cheng, Kai-Wei Chang, Michel Galley, and Jianfeng Gao. MathVista: Evaluating mathematical reasoning of foundation models in visual contexts. In *International Conference on Learning Representations (ICLR)*, 2024.
- Kyle Mahowald, Anna A. Ivanova, Idan A. Blank, Nancy Kanwisher, Joshua B. Tenenbaum, and Evelina Fedorenko. Dissociating language and thought in large language models. *Trends in Cognitive Sciences*, 28(6):517–540, 2024. doi: 10.1016/j.tics.2024.01.011.
- Ahmed Masry, Do Xuan Long, Jia Qing Tan, Shafiq Joty, and Enamul Hoque. ChartQA: A benchmark for question answering about charts with visual and logical reasoning. In *Findings of the Association for Computational Linguistics: ACL 2022*, pages 2263–2279, Dublin, Ireland, 2022. Association for Computational Linguistics.
- OpenAI. GPT-5, 2026. Model card.
- Yujie Qian, Jiang Guo, Zhengkai Tu, Connor W. Coley, and Regina Barzilay. RxnScribe: A sequence generation model for reaction diagram parsing. *Journal of Chemical Information and Modeling*, 63(13):4030–4041, 2023a. doi: 10.1021/acs.jcim.3c00439.
- Yujie Qian, Jiang Guo, Zhengkai Tu, Zhening Li, Connor W. Coley, and Regina Barzilay. MolScribe: Robust molecular structure recognition with image-to-graph generation. *Journal of Chemical Information and Modeling*, 63(7):1925–1934, 2023b. doi: 10.1021/acs.jcim.2c01480.
- Pooyan Rahmanzadehgervi, Logan Bolton, Mohammad Reza Taesiri, and Anh Totti Nguyen. Vision language models are blind: Failing to translate detailed visual features into words. arXiv:2407.06581, 2024.
- Kurt Reidemeister. Elementare Begründung der Knotentheorie. *Abhandlungen aus dem Mathematischen Seminar der Universität Hamburg*, 5:24–32, 1927. doi: 10.1007/BF02952507.
- Zayne Sprague, Fangcong Yin, Juan Diego Rodriguez, Dongwei Jiang, Manya Wadhwa, Prasann Singhal, Xinyu Zhao, Xi Ye, Kyle Mahowald, and Greg Durrett. To CoT or not to CoT? chain-of-thought helps mainly on math and symbolic reasoning. arXiv:2409.12183, 2024.
- Shengbang Tong, Zhuang Liu, Yuexiang Zhai, Yi Ma, Yann LeCun, and Saining Xie. Eyes wide shut? exploring the visual shortcomings of multimodal LLMs. In *Proceedings of the IEEE/CVF Conference on Computer Vision and Pattern Recognition (CVPR)*, 2024.
- Anne M. Treisman and Garry Gelade. A feature-integration theory of attention. *Cognitive Psychology*, 12(1):97–136, 1980. doi: 10.1016/0010-0285(80)90005-5.
- Colin White, Samuel Dooley, Manley Roberts, Arka Pal, Ben Feuer, Siddhartha Jain, Ravid Shwartz-Ziv, Neel Jain, Khalid Saifullah, Sreemanti Dey, Shubh-Agrawal, Sandeep Singh Sandha, Siddhartha Naidu, Chinmay Hegde, Yann LeCun, Tom Goldstein, Willie Neiswanger, and Micah

Goldblum. LiveBench: A challenging, contamination-limited LLM benchmark. arXiv:2406.19314, 2024.

Xiang Yue, Yuansheng Ni, Kai Zhang, Tianyu Zheng, Ruoqi Liu, Ge Zhang, Samuel Stevens, Dongfu Jiang, Weiming Ren, Yuxuan Sun, Cong Wei, Botao Yu, Ruibin Yuan, Renliang Sun, Ming Yin, Boyuan Zheng, Zhenzhu Yang, Yibo Liu, Wenhao Huang, Huan Sun, Yu Su, and Wenhua Chen. MMMU: A massive multi-discipline multimodal understanding and reasoning benchmark for expert AGI. In *Proceedings of the IEEE/CVF Conference on Computer Vision and Pattern Recognition (CVPR)*, 2024.

## A Knot-theory formalism

A *knot* is a smooth embedding  $\phi : S^1 \hookrightarrow S^3$ , considered up to ambient isotopy. Two knots  $K_0, K_1$  are equivalent when there is a continuous family of self-homeomorphisms of  $S^3$  carrying  $K_0$  to  $K_1$ ; the equivalence class is the topological object of interest. A *knot diagram* is the image of  $\phi$  under a generic projection  $S^3 \rightarrow \mathbb{R}^2$  together with a crossing label at each double point recording which strand passes over the other.

The diagram is recorded in a *PD code* (planar diagram code): each crossing contributes a 4-tuple  $(a, b, c, d)$  listing the four arcs that meet at that crossing, read counter-clockwise from the incoming under-arc. The conventions for which arc is listed first and how arcs are numbered differ between libraries; we use Regina’s PD ordering throughout, and the trefoil  $3_1$  in our corpus carries the seed PD code  $[[2, 5, 3, 6], [4, 1, 5, 2], [6, 3, 1, 4]]$ .

**Reidemeister moves and the theorem.** Three local edits act on diagrams without changing the underlying knot: **R1** adds or removes a self-loop (a single new crossing), **R2** adds or removes a bigon (two new crossings), and **R3** slides one strand across a crossing of the other two (crossing count unchanged). Each move has a  $+$  form (add crossings) and a  $-$  form (remove them); R3 is its own inverse. Reidemeister’s theorem [Reidemeister, 1927] states that two diagrams represent the same knot if and only if they differ by a finite sequence of R1, R2, R3 moves. This is the formal handle on which the B-family tasks of the benchmark hang.

**Signature: two senses.** The word *signature* is overloaded in the knot-theory literature. The classical signature  $\sigma(K) \in \mathbb{Z}$  is an integer invariant computed from a Seifert matrix of  $K$ ; we use it only as one of the four classical invariants (Jones, Alexander,  $\sigma$ , determinant) that mutant pairs collide on. The *canonical knot signature* returned by Regina’s `knotSig` [Burton et al., 2024] is a string that canonically identifies the diagram modulo Reidemeister moves; two diagrams of the same knot produce identical `knotSig` strings, and two distinct knots produce different ones, making it a complete invariant in the regime our benchmark touches. Whenever this paper writes “signature” without qualification we mean the Regina `knotSig`.

**Mutant pairs.** A *mutant pair* is a pair of distinct knots that agree on the four classical invariants  $(J_K(t), \Delta_K(t), \sigma(K), \det(K))$ . The smallest example is the Kinoshita–Terasaka pair  $K_{11n34} \neq K_{11n42}$ . Regina’s `knotSig` separates them. Mutant pairs serve as the hardest negatives in the A0 tasks of the benchmark.

## B Corpus construction details

The main text (Section 3) gives the corpus headline: 858,318 PNG renders drawn from 1,951 prime-knot prototypes by random walks of Reidemeister moves. This appendix gives the implementation level so that a reader can rebuild the pipeline or audit its outputs.

**Prototype source.** The 1,951 prototypes are sampled from Regina’s prime-knot tables. Table 3 lists the per-rc counts. For  $rc \leq 11$  we take every prime knot Regina enumerates; at  $rc \in \{12, 13\}$  we sample 200 alternating prototypes per crossing number; at  $rc \in \{14, 15, 16\}$  we sample 150 per rc; at  $rc \in \{17, 18, 19\}$  we sample 100 per rc, drawn from Regina’s **Census** of prime knots with the alternating subclass preferred when both are available. Each prototype carries a seed PD code, its Regina name, its DT code, its classical-signature invariant set, and its canonical **knotSig**.

**Table 3:** Per-rc prototype counts in the corpus. “Available” is the number of prime knots that Regina tabulates at that rc; “sampled” is the number we drew. Below  $rc = 12$  we take every prototype; above we sample to keep wall-clock manageable.

$rc$	Available	Sampled	Alternating share
3	1	1	1.00
4	1	1	1.00
5	2	2	1.00
6	3	3	1.00
7	7	7	1.00
8	21	21	1.00
9	49	49	1.00
10	165	165	1.00
11	552	552	0.66
12	2,176	200	0.62
13	9,988	200	0.60
14	~46k	150	sampled
15	~253k	150	sampled
16	~1.39M	150	sampled
17	sampled	100	sampled
18	sampled	100	sampled
19	sampled	100	sampled
total	—	1,951	

**Random-walk energy function.** Each (prototype, chirality) is the seed of 128 independent random walks. A walk is a Metropolis–Hastings chain over PD codes whose proposal distribution is the six Reidemeister-move primitives in Table 4. The acceptance ratio is biased by an energy

$$E(D) = \lambda_{\text{size}} |D| + \lambda_{\text{tiny}} (N_{1\text{-face}}(D) + 0.5 N_{2\text{-face}}(D)), \quad (1)$$

where  $|D|$  is the crossing count of  $D$ , and  $N_{k\text{-face}}(D)$  counts  $k$ -faces in the planar dual of  $D$ :  $N_{1\text{-face}}$  is the number of self-loops (kinks) and  $N_{2\text{-face}}$  the number of bigons (R2 patches). We set  $\lambda_{\text{size}} = 0.05$  and  $\lambda_{\text{tiny}} = 1.0$ . The Metropolis acceptance is  $\min(1, e^{-\beta \Delta E})$  with  $\beta = 1$ . The size term keeps walks from running off to thousand-crossing diagrams; the small-face terms keep walks from accumulating visually pathological features that hurt downstream rendering. Two hard rejects also fire: if the proposal increases the crossing count past  $|D'| > 30$  the move is rejected outright (the corpus’s

complexity ceiling), and if a topology check  $\text{sig}(D') \neq \text{sig}(D_0)$  ever triggers the walk is aborted (the topology check is a sanity rather than an expected behaviour: a faithful R-move implementation should never change the canonical signature, and this guard has not fired on any production walk).

**Table 4:** R-move primitives proposed by the random walk and the weights with which they are sampled. “flype” is implemented as an R3 swap that is sound by Reidemeister’s theorem; in the trajectory analysis it should be aggregated with R3.

Move	Weight	Implementation
R3	0.40	<code>Link.r3</code>
R2 <sup>+</sup>	0.20	<code>Link.r2(uA, uS, lA, lS)</code>
R2 <sup>-</sup>	0.15	<code>Link.r2(crossing)</code>
R1 <sup>+</sup>	0.10	<code>Link.r1(arc, side, sign)</code>
R1 <sup>-</sup>	0.10	<code>Link.r1(crossing)</code>
flype	0.05	implemented as an R3 swap (sound by Reidemeister)

**Walk length, archive, and B0 trajectory store.** Each walk runs for a length sampled uniformly between 80 and 160 steps. The terminal state is laid out and rendered to one PNG; every accepted intermediate state is also archived to JSONL under a per-prototype path keyed by an 8-byte blake2b digest of the prototype id. The archive is roughly 18 GB and contains 256 walks per prototype (chirality  $\times$  walks) at up to 160 steps each. The B-family tasks of the benchmark draw their items from this archive.

**Layout subprocess.** We isolate Sage in a subprocess because spherogram’s CFFI bindings allocate native memory that does not always free cleanly under Python multiprocessing fork; under sustained load this would produce slow, hard-to-trace leaks. The subprocess exposes a JSONL stdin/stdout protocol: the parent process writes one JSON line per PD code on stdin, and the child writes one JSON line per laid-out diagram on stdout. The subprocess is restarted every 1,024 layouts to bound resident memory.

**Rasterization.** Layouts are rasterised to 800 $\times$ 800 PNGs via `cairo`. Routing is forced to straight polylines with clean over/under breaks at crossings; curved routings misalign on diagrams with  $\geq 4$  crossings (see KnotBench feedback memos). Per-render style is randomised: a 7-colour palette (one of the seven uniformly), a 12-bin in-plane rotation (one of the twelve uniformly), and a texture (solid or rope-twist, 50/50 by construction). Stroke width and the over/under gap size are also randomised within fixed intervals.

**Visual lint.** Some random layouts produce visually broken renders even when the PD code is valid (overlapping strands, near-collinear arcs). We filter these with two metrics. The *overlap ratio* is  $\max(\text{DT})/p_{99}(\text{DT})$ , where DT is the distance transform of the rendered strand mask; values much greater than 1 indicate that the strand fattens into a blob. The *parallel-close score* is the fraction of skeleton pixels that are within 5 pixels of a different strand. We discard a render if its overlap ratio exceeds 1.5 or its parallel-close score exceeds 0.05. In our production run, 4,316/862,634  $\approx$  0.5% of attempts failed lint; the surviving 858,318 form the corpus.

**Style coverage.** The 7-colour palette receives  $14.0\% \pm 0.4\%$  of renders per colour. The 12-bin rotation histogram is uniform within  $\pm 0.4\%$ . Texture is 50/50 (solid vs rope-twist) by construction;

chirality is 50/50 (original vs mirror) by construction. These four uniformity statements imply that the random walk does not bias the visual style space and that no A-family task is solvable by a stylistic shortcut.

**Reproducibility.** The corpus is byte-deterministic at the PD-code level. Each random-walk seed is a 64-bit value derived from a blake2b digest of (`prototype_id` || `chirality` || `‘walk’`) plus  $9973 \cdot \text{walk\_idx}$ ; rerunning the pipeline with the same seeds reproduces the manifest’s PD codes exactly. PNG byte-equality holds only when `cairo`, `pango`, and the system fonts are pinned to the versions we used; we record those versions in the release lockfile alongside SHA-256 hashes of every frozen artifact. The eval set `eval_items.jsonl` hashes to `a7a72c63...`, with the full list in the released manifest.

## C Worked example: a single random walk

To make the pipeline concrete, this appendix walks through the first ten Metropolis–Hastings steps of one production-style walk on the trefoil seed prototype `3a_1`. The seed PD code is

$$D_0 = [[2, 5, 3, 6], [4, 1, 5, 2], [6, 3, 1, 4]],$$

with  $|D_0| = 3$ , canonical signature  $\text{sig}(D_0) = \text{dabcabcv-}$ ,  $N_{1\text{-face}}(D_0) = 0$ ,  $N_{2\text{-face}}(D_0) = 0$ , so  $E(D_0) = 0.05 \cdot 3 + 0 = 0.15$ . The proposal distribution is given by Table 4. We record at each step the proposal type, the candidate diagram’s crossing count and small-face counts, the energy delta  $\Delta E$ , the Metropolis acceptance probability  $\min(1, e^{-\Delta E})$ , the uniform random draw used to accept or reject, and the post-step state.

The ten steps below are illustrative rather than verbatim from one specific archived walk: archived walks contain many R3 moves that do not change  $|D|$  or visibly change  $E$ , and the early-walk profile we show would be quickly buried in such transitions. The energy arithmetic and acceptance rule are exact.

- Step 1.** Propose **R1**<sup>+</sup>. Candidate adds one self-loop, so the candidate has  $|D'| = 4$ ,  $N_{1\text{-face}} = 1$ ,  $N_{2\text{-face}} = 0$ .  $E(D') = 0.05 \cdot 4 + 1.0 \cdot 1 = 1.20$ .  $\Delta E = 1.20 - 0.15 = 1.05$ . Acceptance probability  $\min(1, e^{-1.05}) \approx 0.350$ . The walk draws  $u = 0.62$  and *rejects*. State unchanged:  $D_1 = D_0$ ,  $E(D_1) = 0.15$ .
- Step 2.** Propose **R2**<sup>+</sup>. Candidate adds one bigon, so  $|D'| = 5$ ,  $N_{1\text{-face}} = 0$ ,  $N_{2\text{-face}} = 1$ .  $E(D') = 0.05 \cdot 5 + 0.5 \cdot 1 = 0.75$ .  $\Delta E = 0.60$ . Acceptance probability  $e^{-0.60} \approx 0.549$ . Draws  $u = 0.18$  and *accepts*.  $D_2$  has  $|D_2| = 5$  and one bigon;  $E(D_2) = 0.75$ .
- Step 3.** Propose **R3**. Candidate keeps  $|D'| = 5$  and removes the bigon by sliding a strand:  $N_{2\text{-face}}$  may drop to 0 but is not guaranteed to. Assume it does in this draw:  $E(D') = 0.25$ ,  $\Delta E = -0.50$ , acceptance probability 1. Accept.  $D_3 = D'$ ,  $E(D_3) = 0.25$ .
- Step 4.** Propose **R2**<sup>+</sup>. Adds a fresh bigon.  $|D'| = 7$ ,  $N_{1\text{-face}} = 0$ ,  $N_{2\text{-face}} = 1$ .  $E(D') = 0.85$ ,  $\Delta E = 0.60$ ,  $p = 0.549$ ,  $u = 0.71$ , *reject*.  $D_4 = D_3$ .
- Step 5.** Propose **R3**. No small-face change at the swap site.  $E(D') = 0.25$ ,  $\Delta E = 0$ ,  $p = 1$ , *accept*.  $D_5 = D'$  with  $|D_5| = 5$ .
- Step 6.** Propose **R1**<sup>+</sup>.  $|D'| = 6$ ,  $N_{1\text{-face}} = 1$ .  $E(D') = 1.30$ ,  $\Delta E = 1.05$ ,  $p \approx 0.350$ ,  $u = 0.91$ , *reject*.  $D_6 = D_5$ .

**Step 7.** Propose **R1<sup>-</sup>**. Cannot remove a self-loop because  $D_5$  has none; the move is structurally invalid and the proposal is dropped (*rejected without energy computation*).  $D_7 = D_6$ .

**Step 8.** Propose **R3**. Accept with  $\Delta E = 0$  as before.  $D_8$  at  $|D_8| = 5$ .

**Step 9.** Propose **R2<sup>+</sup>**.  $|D'| = 7$ ,  $N_{2\text{-face}} = 1$ ,  $E(D') = 0.85$ ,  $\Delta E = 0.60$ ,  $p = 0.549$ ,  $u = 0.34$ , *accept*.  $D_9$  now has one bigon and seven crossings.

**Step 10.** Propose **R3**. The R3 site happens to share a face with the new bigon and removes it;  $|D_{10}| = 7$ ,  $N_{2\text{-face}} = 0$ ,  $E(D_{10}) = 0.35$ ,  $\Delta E = -0.50$ , *accept*.

After ten steps the walker has explored four distinct diagrams, the crossing count has wandered from 3 to 7 and back to 7, and the bigon count has cycled  $0 \rightarrow 1 \rightarrow 0 \rightarrow 1 \rightarrow 0$ . The canonical signature is unchanged at every accepted state. A production walk runs 80 to 160 such steps and ends at a diagram between roughly  $|D| = 8$  and  $|D| = 25$  depending on the energy landscape; Fig. 3 in Section 3 shows two such terminal renders. Trajectory archives store every accepted state, so the B0 task’s item generator can sample consecutive pairs  $(D_t, D_{t+1})$  at arbitrary depths into a walk.

## D Reidemeister moves illustrated

The three Reidemeister moves are the only edits that compose to generate all diagrams of a fixed knot, and the directed forms  $R1^\pm$ ,  $R2^\pm$ ,  $R3$  are the six labels used by the B0 task. The five directed forms break down as follows:  $R1^+$  adds a single self-loop;  $R1^-$  removes one;  $R2^+$  adds a bigon;  $R2^-$  removes one;  $R3$  slides a strand across a crossing of the other two and preserves the crossing count.  $R3$  is its own inverse, which is why the B0 label set is six rather than seven (no  $R3^+$  /  $R3^-$  distinction). A move is locally identified by reading the diagram in a disk around the affected region; outside the disk both diagrams agree. The B0 task asks the model to identify which of the six moves (or NOT-CONNECTED) transforms  $D_t$  into  $D_{t+1}$ , where  $D_t$  and  $D_{t+1}$  are consecutive accepted states of an archived walk.

## E The 14 evaluation prompts in full

This appendix prints the verbatim text of every task’s prompt template, as extracted from `phase2.eval/eval_run/prompts.py`. The system message is identical across all 14 tasks and is shown once below. For each task the user message template is shown in a boxed block; where the task consumes a rendered diagram, the position of the inserted PNG is marked `<<IMAGE>>`; where it consumes a PD code, the PD code is formatted as one bracketed list on a single line. PD-code formatting uses Regina ordering throughout.

**System message (shared).**

You are a topology expert evaluating knot diagrams. Read each question carefully. Always finish your answer with a line in the EXACT format requested --- do not add explanation after the answer line.

**A0.I — same knot? (images).**

You are given two knot diagrams, labeled DIAGRAM A and DIAGRAM B.  
Are DIAGRAM A and DIAGRAM B drawings of the SAME knot (i.e., topologically equivalent)?  
Answer ONLY 'yes' or 'no' on the LAST line, exactly. Format your final line as:  
ANSWER: yes or ANSWER: no  
DIAGRAM A: <<IMAGE A>>  
DIAGRAM B: <<IMAGE B>>

**A0\_S — same knot? (PD codes).**

You are given two knot diagrams, labeled DIAGRAM A and DIAGRAM B.  
Are DIAGRAM A and DIAGRAM B drawings of the SAME knot (i.e., topologically equivalent)?  
Answer ONLY 'yes' or 'no' on the LAST line, exactly. Format your final line as:  
ANSWER: yes or ANSWER: no  
DIAGRAM A (PD code):  
<<PD A>>  
DIAGRAM B (PD code):  
<<PD B>>

**A1\_I — same chirality, given same knot? (images).**

You are given two knot diagrams, labeled DIAGRAM A and DIAGRAM B. Both diagrams are guaranteed to be drawings of the same knot.  
DIAGRAM A and DIAGRAM B are drawings of the same knot. Are they drawn with the SAME chirality (handedness)? Two diagrams have the same chirality iff one is NOT the mirror image of the other.  
Answer ONLY 'yes' or 'no' on the LAST line, exactly. Format your final line as:  
ANSWER: yes or ANSWER: no  
DIAGRAM A: <<IMAGE A>>  
DIAGRAM B: <<IMAGE B>>

**A1\_S — same chirality, given same knot? (PD codes).**

You are given two knot diagrams, labeled DIAGRAM A and DIAGRAM B. Both diagrams are guaranteed to be drawings of the same knot.  
DIAGRAM A and DIAGRAM B are drawings of the same knot. Are they drawn with the SAME chirality (handedness)? Two diagrams have the same chirality iff one is NOT the mirror image of the other.  
Answer ONLY 'yes' or 'no' on the LAST line, exactly. Format your final line as:  
ANSWER: yes or ANSWER: no  
DIAGRAM A (PD code):  
<<PD A>>  
DIAGRAM B (PD code):  
<<PD B>>

**A2\_I — same crossing count, given same knot+chirality? (images).**

You are given two knot diagrams, labeled DIAGRAM A and DIAGRAM B. Both diagrams represent the same knot, drawn with the same chirality.  
DIAGRAM A and DIAGRAM B depict the same knot drawn with the same chirality. Do they have the SAME number of crossings?  
Answer ONLY 'yes' or 'no' on the LAST line, exactly. Format your final line as:  
ANSWER: yes or ANSWER: no  
DIAGRAM A: <<IMAGE A>>  
DIAGRAM B: <<IMAGE B>>

**A2.S — same crossing count, given same knot+chirality? (PD codes).**

You are given two knot diagrams, labeled DIAGRAM A and DIAGRAM B. Both diagrams represent the same knot, drawn with the same chirality.  
DIAGRAM A and DIAGRAM B depict the same knot drawn with the same chirality. Do they have the SAME number of crossings?  
Answer ONLY 'yes' or 'no' on the LAST line, exactly. Format your final line as:  
ANSWER: yes or ANSWER: no  
DIAGRAM A (PD code):  
<<PD A>>  
DIAGRAM B (PD code):  
<<PD B>>

**A3.I — same canonical PD, given same bucket? (images).**

You are given two knot diagrams, labeled DIAGRAM A and DIAGRAM B. Both diagrams represent the same knot, with the same chirality, with the same crossing count.  
DIAGRAM A and DIAGRAM B are drawings of the same knot, drawn with the same chirality, with the same number of crossings. Do they represent the SAME canonical planar diagram (i.e., are they identical as diagrams up to relabeling of strands)?  
Answer ONLY 'yes' or 'no' on the LAST line, exactly. Format your final line as:  
ANSWER: yes or ANSWER: no  
DIAGRAM A: <<IMAGE A>>  
DIAGRAM B: <<IMAGE B>>

**A3.S — same canonical PD, given same bucket? (PD codes).**

You are given two knot diagrams, labeled DIAGRAM A and DIAGRAM B. Both diagrams represent the same knot, with the same chirality, with the same crossing count.  
DIAGRAM A and DIAGRAM B are drawings of the same knot, drawn with the same chirality, with the same number of crossings. Do they represent the SAME canonical planar diagram (i.e., are they identical as diagrams up to relabeling of strands)?  
Answer ONLY 'yes' or 'no' on the LAST line, exactly. Format your final line as:  
ANSWER: yes or ANSWER: no  
DIAGRAM A (PD code):  
<<PD A>>  
DIAGRAM B (PD code):  
<<PD B>>

**B0\_I — which R-move connects two diagrams? (images).**

You are given two knot diagrams, DIAGRAM\_T and DIAGRAM\_T1, that are claimed to be consecutive steps of a Reidemeister-move sequence on the same underlying knot.

Which Reidemeister move (if any) transforms DIAGRAM\_T into DIAGRAM\_T1?

Choices:

R1+ add one self-loop (one new crossing)

R1- remove one self-loop (delete one crossing)

R2+ add one bigon (two new crossings)

R2- remove a bigon (delete two crossings)

R3 triangle move (3 strands swap, no crossing-count change)

NOT-CONNECTED the two diagrams are NOT connected by a single R-move

Answer ONLY one of {R1+, R1-, R2+, R2-, R3, NOT-CONNECTED} on the LAST line, exactly as:

ANSWER: <choice>

DIAGRAM\_T: <<IMAGE T>>

DIAGRAM\_T1: <<IMAGE T+1>>

**B0\_S — which R-move connects two diagrams? (PD codes).**

You are given two knot diagrams, DIAGRAM\_T and DIAGRAM\_T1, that are claimed to be consecutive steps of a Reidemeister-move sequence on the same underlying knot.

Which Reidemeister move (if any) transforms DIAGRAM\_T into DIAGRAM\_T1?

Choices:

R1+ add one self-loop (one new crossing)

R1- remove one self-loop (delete one crossing)

R2+ add one bigon (two new crossings)

R2- remove a bigon (delete two crossings)

R3 triangle move (3 strands swap, no crossing-count change)

NOT-CONNECTED the two diagrams are NOT connected by a single R-move

Answer ONLY one of {R1+, R1-, R2+, R2-, R3, NOT-CONNECTED} on the LAST line, exactly as:

ANSWER: <choice>

DIAGRAM\_T (PD code):

<<PD T>>

DIAGRAM\_T1 (PD code):

<<PD T+1>>

**C0 — count crossings.**

Count the number of crossings in this knot diagram.

Answer with a single integer on the LAST line:

ANSWER: <integer>

<<IMAGE>>

**C1 — DT-code transcription.**

```
This is a knot diagram. Provide the alphabetical Dowker-Thistlethwaite (DT) code
for it.
Format: a string of lowercase letters of length n (where n is the number of
crossings). Use the standard alphabetical DT convention.
Answer with the DT string ONLY on the LAST line:
ANSWER: <dt-string>
<<IMAGE>>
```

### D0 — does this PD code describe this image?

```
You are given an image of a knot diagram and a PD code.
Question: Does the PD code describe THIS image?
Answer ONLY 'yes' or 'no' on the LAST line, exactly:
ANSWER: yes or ANSWER: no
Image: <<IMAGE>>
PD code to verify:
<<PD>>
```

### D1 — which of 4 PD codes describes this image?

```
You are given an image of a knot diagram and 4 candidate PD codes labeled A, B, C,
D.
Question: Which PD code correctly describes the diagram in the image?
Option A:
<<PD A>>
Option B:
<<PD B>>
Option C:
<<PD C>>
Option D:
<<PD D>>
Answer ONLY one letter A, B, C, or D on the LAST line, exactly:
ANSWER: <letter>
<<IMAGE>>
```

## F Scoring rules in detail

Scoring is strict and string-based. For each (item, response) the scorer extracts the last `ANSWER:` ... line, normalises it, and compares against the ground-truth label. If no `ANSWER:` line is present the scorer falls back to the last non-empty line. If no non-empty line is present the response is recorded as empty and is wrong by definition.

**Binary tasks (A0–A3, D0).** The ANSWER text is lower-cased and stripped of trailing punctuation. A short whitelist normalises to `yes` or `no`: the set `{yes, y, true, same, matching}` maps to `yes` and the set `{no, n, false, different, not}` maps to `no`; tokens starting with `yes` or `no` fall back to those tokens. Any unparseable answer is recorded as `None` and is wrong.

**B0 (R-move multi-class).** The ANSWER text is upper-cased and stripped of whitespace and of parentheses. The valid choices are `{R1+, R1-, R2+, R2-, R3, NOT-CONNECTED}`; the variants `NOTCONNECTED`, `NOT_CONNECTED`, and `NOT CONNECTED` all collapse to `NOT-CONNECTED`. Any un-

parseable string is recorded as `None`. The scorer does *not* accept `R1plus`, `R1^+`, or other notations the prompt did not advertise; the prompt is explicit about the six-token vocabulary.

**C0 (integer crossing count).** The ANSWER text is searched for the first signed integer using the regex `-?\d+`. The integer is compared to the ground-truth crossing count  $n_x$ .

**C1 (DT code transcription).** The ANSWER text is lower-cased and stripped of common trailing punctuation including quotation marks and backticks. The first scoring tier is strict string match against the ground-truth DT code. A second permissive tier, run as a separate post-pass, decodes the model’s string via Regina’s `Link.fromDT(...).knotSig()` and compares the resulting canonical signature to the ground-truth signature; if Regina cannot decode the string, the item remains scored as wrong. Headline C1 numbers in the main text are the strict tier; the permissive recovery is reported in Section 5.

**D1 (4-way MCQ).** The ANSWER text is upper-cased and stripped; the first character in `{A, B, C, D}` is taken as the answer. The scorer does not attempt to recover from a model that emits the full PD code instead of a letter; such responses are recorded as `None`.

**Empty responses.** A response with no extractable answer line and no non-empty fallback line is recorded with `parsed = None` and counted as wrong. On the canonical post-rerun, 0 of 2,000 such empties occurred on `claude-opus-4-7`, 4 on `claude-opus-4-7+thinking`, 0 on `gpt-5`, and 19 on `gpt-5+thinking`; these residual empties are the runs that hit the 64K token ceiling while still emitting reasoning tokens.

## G Per-task narrative reads

Headline per-task accuracies are in Table 5 below; the narratives in this appendix interpret what each task’s per-model profile reveals about the perception–operation gap. The format is the same in every paragraph: task ID, plain-English question, per-model accuracies as a four-tuple ordered (`claude`, `claude+T`, `gpt-5`, `gpt-5+T`), dominant failure mode, and a short reading. Confidence intervals (Wilson 95%) are in Fig. 12; per-stratum gradients are in Fig. 13.

**A0.I — “Are these two images the same knot?” (52.5, 55.0, 47.5, 50.0).** All four models sit at or very close to the binary random baseline. The task asks the broadest equivalence question in the benchmark, and the input strain is correspondingly hardest: the two diagrams may differ in chirality, in crossing count, and in canonical PD even when they share a knot. The dominant failure mode is yes/no near-symmetry under the random-baseline distribution; the per-subtype breakdown (positive items vs mutant negatives vs same-family negatives) shows no model recovers above 60% on any subtype. Mutant negatives are roughly as hard as same-family negatives, which is itself a finding: invariant collisions (Fig. 15) do not buy the model anything because it cannot use the invariants in the first place. The plausible cause is that the A0.I operation requires collapsing visual diversity through a chain of R-moves, and the lineup does not perform that reduction reliably from pixels.

**A0.S — “Are these two PD codes the same knot?” (52.0, 60.0, 61.5, 55.5).** Symbolic input lifts a few points over A0.I but the same near-random ceiling holds. GPT-5 without thinking is the best performer here (61.5%), and thinking does not help; in fact `gpt-5+thinking` falls from

61.5% to 55.5%, the only  $-S$  task on which thinking reverses sign on GPT-5. The dominant failure mode is the same yes/no near-symmetry as in A0.I, with negatives slightly better answered than positives across the lineup. The symbolic prompt does not give the model a handle on “same knot” because the topological test is non-trivial even with PD codes in hand: a solver needs to either compute an invariant or run a sequence of R-moves on the codes, and neither pathway is reliable from the prompt. The reading for the paper’s gap claim is that A0 is hard at every modality because the operation (decide Reidemeister equivalence) is itself hard, not because perception is bad.

**A1.I — “Same chirality, given same knot? (images)” (46.0, 47.0, 48.0, 49.0).** All four models sit below random by 1–4 points. Chirality detection from pixels requires reading the over/under marking at multiple crossings consistently across the diagram, then deciding whether the global handedness pattern is preserved between the two images. The amphichiral-positive items (20% of A1, where the diagram and its mirror are the same knot up to ambient isotopy) further break a naive “mirror  $\Rightarrow$  flipped” heuristic because in these items both “orig” and “mirror” renders should be labelled “yes”. The dominant failure mode is a yes/no flip near the random axis with no per-subtype structure: the model neither uses chirality cues from over/under marks nor exploits the amphichiral whitelist. Thinking does not move the task. The operation here is perceptual rather than topological, and it collapses in a way that does not show up on the symbolic variant.

**A1.S — “Same chirality, given same knot? (PD codes)” (65.0, 92.0, 44.0, 69.0).** This is the largest reasoning-mode lift on Claude in the benchmark (+27pt). claude+thinking reaches 92% and gpt-5+thinking reaches 69%; non-thinking GPT-5 sits at 44%, below random. Chirality flips correspond to a sign-symmetric relabelling of the PD code that thinking-mode reasoning can work out from the symbolic input, typically by tracing the over/under pattern around a small loop and checking whether the trace direction is preserved. The dominant failure mode for the non-thinking models is a yes/no flip on items where the relabelling spans many crossings; thinking-mode reasoning closes that gap on Claude and partially on GPT-5. The amphichiral-positive subtype is the hard part of the task because its “correct” label is “yes” on both orig-vs-mirror and orig-vs-orig pairs, which contradicts the heuristic that mirrored PD codes are always answered “no”. A1.S is one of the tasks where reasoning tokens convert directly into accuracy.

**A2.I — “Same crossing count? (images)” (67.0, 65.0, 45.0, 50.0).** Counting two crossing counts and comparing them is the simplest operation in the benchmark, and Claude solves it from images at about 67% while GPT-5 sits at chance. Thinking does not help either vendor; in fact claude+thinking falls 2 points on the task. The dominant failure mode is the C0-style mis-count carried into the comparison: when the model cannot reliably count a single diagram, it cannot reliably compare two, and the comparison fails in proportion to the harder of the two counts. The cross-vendor gap (Claude 67% vs gpt-5 45%) is one of the largest in the image-only column and suggests vendor-specific counting differences that the benchmark exposes. Notably the task does not require exact counts on either side, only that the two counts agree, so a model whose counts are biased but consistently biased could still score above chance; the cross-vendor gap then reads as a consistency gap rather than an absolute-accuracy gap.

**A2.S — “Same crossing count? (PD codes)” (97.0, 99.0, 96.0, 100.0).** A2.S is a sanity check: each PD code is a list of 4-tuples whose length is the crossing count, so the task reduces to comparing two list lengths. All four models score  $\geq 96\%$  and gpt-5+thinking hits 100%. The

task confirms that the prompt template and the scoring pipeline are not themselves broken; it is otherwise uninformative.

**A3\_I — “Same canonical PD, given same bucket? (images)” (90.5, 90.5, 63.0, 74.5).**

A3\_I is the strongest image-only task in the benchmark and shows the widest cross-vendor gap among above-random tasks. Both Claude variants reach 90.5% with thinking adding nothing; GPT-5 sits at 63% and lifts to 74.5% with thinking. The task pairs two diagrams that share prototype, chirality, and crossing count, so the discriminating feature is the canonical PD itself; positives use the same canonical PD (and differ only in random-walk diversification that preserves the canonical form), while negatives differ in canonical PD despite agreeing on everything else. The dominant failure mode on GPT-5 is a yes-class flip: a positive item is answered “no” when the visual relabelling crosses the encoder’s patch boundaries. The plausible cause of the cross-vendor gap is a difference in how the two vision encoders preserve fine over/under structure across these relabellings, and the gap does not close under thinking because the failure happens before the reasoning trace starts (Section K shows representative one-token responses).

**A3\_S — “Same canonical PD, given same bucket? (PD codes)” (50.0, 50.0, 48.0, 99.0).**

gpt-5+thinking solves the task almost perfectly (99%) while the three other configurations sit at chance. The task reduces to a graph-isomorphism-style test on small labelled graphs (each PD code is a list of 4-tuples), and the reasoning trace on gpt-5+thinking is apparently able to perform that test by relabelling arcs and comparing the resulting crossing 4-tuples as multisets. claude+thinking stays at chance, the only  $-S$  task where Claude does not gain from reasoning. The dominant failure mode on the three near-random configurations is a yes/no flip with no discriminative structure across the two A3\_S subtypes (`same_wl_hash` vs `different_wl_hash`); the models are not running the relabelling test at all. The asymmetry is the cleanest task-level evidence of a divergence in how the two thinking modes use their token budget: GPT-5’s high-reasoning chain finds the relabelling, Claude’s adaptive thinking does not. We return to this asymmetry in the discussion of reasoning effect in Section 5.

**B0\_I — “Which R-move connects  $D_t$  and  $D_{t+1}$ ? (images)” (29.5, 32.5, 17.0, 21.0).**

All four models score well below the 6-way random baseline of  $\sim 30\%$  on the image variant. gpt-5 collapses to 17%, well below random, and gpt-5+thinking lifts by only 4 points to 21%. The per-class breakdown in Fig. 9 shows the dominant failure mode: gpt-5 emits R3 on a large majority of items and scores  $\sim 84\%$  on the R3 class while scoring  $<30\%$  on every other class. Because R3 is the most frequent label in the trajectory archive (the walk weights in Table 4 give R3 the largest mass), an always-R3 shortcut scores reasonably on the conditional distribution of R3 items and poorly on everything else; the aggregate accuracy then sits at the always-R3 prior rate, which is below random. The task requires mental simulation (try each candidate move on  $D_t$  and check whether it produces  $D_{t+1}$ ) and that operation fails from pixels. The NOT-CONNECTED class is a useful diagnostic against the shortcut because no R-move generates NOT-CONNECTED, yet B0\_I NOT-CONNECTED items score under 25% on every model. B0\_I is the canonical task against which the perception–operation gap is measured.

**B0\_S — “Which R-move connects  $D_t$  and  $D_{t+1}$ ? (PD codes)” (84.0, 84.0, 41.0, 88.0).**

With the PD codes given directly, three of four configurations score above 80%. Both Claude variants reach 84% (thinking does not move them) and gpt-5+thinking reaches 88% with a +47 point lift over the non-thinking GPT-5. The dominant failure mode on non-thinking GPT-5 is the same always-R3

shortcut as on B0\_I, visible in the qualitative pair where gpt-5 emits NOT-CONNECTED on an R1+ item without analysis; thinking-mode reasoning removes the shortcut on the symbolic variant by actually computing the crossing-count delta and identifying the self-loop. The B0\_S operation reduces to (i) compute  $|D_{t+1}| - |D_t|$ , (ii) check whether a self-loop or bigon was added or removed by looking at the PD code’s 4-tuples, and (iii) emit the matching label. All three sub-operations are reliable when the codes are in the prompt. B0 is the canonical example of the perception–operation split in the benchmark: when the structure is given, the operation works; when the structure has to come from pixels, it does not.

**C0 — “How many crossings in this diagram?” (9.0, 14.0, 8.0, 11.0).** Strict-match crossing-count accuracy collapses past  $n_x \approx 10$ . Figure 10 shows the per- $n_x$  curve: all four models are above 50% at  $n_x = 8$ , drop sharply through  $n_x \in [10, 14]$ , and approach chance by  $n_x = 17$ . The dominant failure mode is a  $\pm 1$  to  $\pm 3$  miscount that the strict integer match rejects; under a  $\pm 1$  tolerance the accuracy roughly doubles but the qualitative collapse remains. The corpus uses orthogonal routing so that each crossing is rendered as an unambiguous over/under glyph; the task is not asking the model to disambiguate visually fragile crossings, only to count them. C0 is the simplest perceptual operation in the benchmark (output one integer) and it is also the task with the lowest absolute accuracy after C1. Thinking-mode reasoning lifts both vendors by 3–5 points and does not change the high-complexity collapse. The reading is that VLMs cannot count crossings in dense diagrams, which is consistent with the chart-and-shape counting failures reported by Rahmanzadehgervi et al. [2024]; here the “what to count” is unambiguous and the failure cleanly localises to the counting operation itself.

**C1 — “What is the DT code of this diagram?” (0.0, 0.0, 0.0, 0.0).** Strict-match DT-code accuracy is zero across all four models. Under the permissive Regina post-pass that decodes the model’s string as a DT code and checks the canonical signature, gpt-5+thinking recovers 4 of 100 items and the other three remain at zero. The dominant failure mode is the production of a string that is either truncated, has wrong length, or is a plausible-looking DT-style alphabetical sequence with no relation to the diagram (the qualitative examples in Section K include `abcde` on a 4-crossing diagram whose DT code is `bcda`). A secondary failure mode is explicit refusal: gpt-5 (no thinking) on item C1\_0009 declines with an explanation that “DT codes depend on over/under crossing information and consistent orientation . . .”, which the strict scorer counts as wrong but which reads as a more honest signal than a confabulated string. C1 is the task that most cleanly isolates the perception-to-symbol direction of the gap: the model is given one diagram and asked for its symbolic fingerprint, and current VLMs do not produce that fingerprint, with or without thinking, under either scoring rule.

**D0 — “Does this PD code describe this image?” (50.5, 47.0, 50.0, 58.0).** D0 sits at random for three of four models, with gpt-5+thinking slightly above. The task has a systematic “no” bias (Fig. 11): matching (positive-class) items receive 0–16% “yes” answers across models, and same-task mismatches receive 86–100% “no” answers. The class-aware reading is that the models do well on negatives by defaulting to “no” and poorly on positives by also defaulting to “no”; in expectation the two biases cancel near 50%. The dominant failure mode is a strong refusal-like prior that rejects valid matches; this prior is arguably calibrated, because verifying a PD code against an image requires recovering the PD code from pixels and comparing the two codes, and that pipeline inherits the C1 failure. When the model cannot verify a match it returns the safer answer. The qualitative pair in Section K shows claude-opus-4-7+thinking solving a negative (a

self-loop crossing in the PD code has no visual counterpart) and failing on a positive (the model abandons a 17-crossing count and answers “no”), which is the canonical shape of D0 error.

**D1 — “Which of these 4 PD codes describes this image?” (32.5, 35.5, 26.0, 30.5).** D1 is the multiple-choice variant of D0 and sits at or just above the 25% random baseline for all models. Thinking lifts both vendors by 3–5 points but does not produce a solver. The dominant failure mode is option-letter near-uniformity (Fig. 17): when the model cannot recover the PD code from the image it cannot rank the four options on content, so the choice is approximately random. The distractor design is the same-task mismatch construction used in D0 negatives (same prototype, same chirality, same crossing count, different canonical PD), so the four options share their classical invariants by construction. A model that decides D1 by invariants alone is therefore guessing. D1 is the strongest indictment of cross-modal grounding in the benchmark because the multiple-choice form gives the model the answer set explicitly — the PD code does not have to be produced, only matched — and the models still cannot use it. The reasoning lift on D1 is smaller than on B0\_S because the operation D1 demands (rank four PD codes against one image) is the inverse of the C1 operation (produce a PD code from one image) and inherits its failure in equal measure.

## H Per-task full results table

Table 5 reports per-(task, model) accuracy on the canonical post-rerun. Wilson 95% confidence intervals and per-task  $n_x$  gradients are in Fig. 12 and Fig. 13.

**Table 5:** Per-(task, model) accuracy (%) on the full evaluation set.

Task	N	Claude	Claude+T	GPT-5	GPT-5+T
A0_I	200	52.5	55.0	47.5	50.0
A0_S	200	52.0	60.0	61.5	55.5
A1_I	100	46.0	47.0	48.0	49.0
A1_S	100	65.0	92.0	44.0	69.0
A2_I	100	67.0	65.0	45.0	50.0
A2_S	100	97.0	99.0	96.0	100.0
A3_I	200	90.5	90.5	63.0	74.5
A3_S	100	50.0	50.0	48.0	99.0
B0_I	200	29.5	32.5	17.0	21.0
B0_S	100	84.0	84.0	41.0	88.0
C0	100	9.0	14.0	8.0	11.0
C1	100	0.0	0.0	0.0	0.0
D0	200	50.5	47.0	50.0	58.0
D1	200	32.5	35.5	26.0	30.5
Mean		51.65	54.60	43.00	52.25

## I Supplementary figures

This appendix collects supplementary figures that support the per-task narratives in Section G. Each caption is self-contained so the figure can be read without the main text.

## J Limitations table

Table 6 lists every limitation we acknowledge in Section 6 with a one-line description, a severity tag (low / medium / high), and the mitigation (or non-mitigation) applied in the paper. The severity tag is calibrated against the benchmark’s headline claim: the perception–operation gap. A “high” limitation is one that could plausibly invalidate a specific claim if reviewers pushed on it; a “low” limitation is a known artefact of scale or scope that we report for completeness.

**Table 6:** Compact view of paper limitations. Severity is calibrated against the gap claim, not against the benchmark’s secondary ranking value. Mitigation is either applied (M) or explicitly deferred (D); “M” rows are the ones where the limitation does not bind on a headline claim.

Limitation	Severity	Mitigation
Test split holds 18 unique mutant pairs (mathematical floor over 98 mutant components); each pair appears up to 4 times across renderings.	medium	M. We report A0 mutant accuracy per-pair and per-rendering and flag the per-pair figure as the conservative read.
L1 ( $rc \leq 7$ ) holds $\sim 24$ records in test; 13 of 14 tasks skip L1.	low	M. Stratification is by $n_x$ bins $\{8-10, 11-13, 14-16, 17-20\}$ for the L2-L3+ regime; L1 is folded into the lowest bin with a flag where it appears.
“flype” is implemented as an R3 swap during walks (5% of moves).	low	M. Analyses aggregate flype counts with R3; the implementation is sound by Reidemeister.
B0 NOT-CONNECTED has $\sim 1\%$ theoretical false-positive risk: a five-step-apart pair could in principle be connected by a single R-move.	low	M. The 1% bound is reported with the B0 results; no observed false positive in spot-checks of NOT-CONNECTED items.
The Weisfeiler–Lehman hash used in A3 negatives is a canonical fingerprint, not a graph-isomorphism invariant.	low	M. Hashes are computed on the canonicalised manifest; the audit log <code>wl_audit.txt</code> certifies the canonicalisation.
Mutant detection uses $(J, A, \sigma, \det)$ collisions; Khovanov homology is omitted (computational cost at $rc \geq 17$ ).	medium	D. Khovanov-based mutant separation is a natural extension.
The A1 amphichiral whitelist is limited to $rc \leq 10$ .	low	M. A1 items with amphichiral positives at $rc > 10$ are not used as positives; the subtype breakdown is reported.
Two-vendor lineup (Anthropic and OpenAI); Gemini and open-weights baselines are absent.	medium	D. Adding Gemini and a large open-weights model is the highest-priority extension.

## K Qualitative examples: correct vs incorrect

Aggregate per-task accuracy hides what the failure looks like at the response level. This appendix shows four pairs of verbatim model outputs (one correct and one incorrect per task) drawn from the canonical results JSONL files. The pairs were selected by sampling from the per-task records and picking the first response in each class with a substantive (non-one-token) output, then checking that the response illustrates the task’s dominant failure mode.

**B0\_S** — which R-move connects two PD codes. On B0\_S, claude-opus-4-7+thinking solves item B0\_S\_0006 correctly: the ground truth is  $R1^+$  and the model’s reasoning isolates the self-loop crossing and matches the label.

<b>B0_S_0006</b> ground truth $R1^+$ model: $R1^+$ CORRECT <i>Looking at the crossing counts: DIAGRAM_T has 13 crossings, DIAGRAM_T1 has 14 crossings (one more). DIAGRAM_T1 contains crossing [22, 22, 23, 21], which has a repeated arc label (22) — a self-loop / kink. The rest of the diagram corresponds (with relabeled arcs) to DIAGRAM_T. This is the addition of one self-loop (one new crossing).</i> ANSWER: $R1^+$
---

On B0\_S\_0000 the same family of reasoning is misapplied by gpt-5 (no thinking), which emits NOT-CONNECTED without analysis:

<b>B0_S_0000</b> ground truth $R1^+$ model: NOT-CONNECTED WRONG <i>NOT-CONNECTED</i> ANSWER: NOT-CONNECTED
--

The contrast is the running theme of B0: the operation is doable from a PD code with a few sentences of reasoning, and it is not doable when the model emits its answer before reasoning. The B0\_I parallel is harsher because the perception step is itself in the loop.

**C1** — DT-code transcription. C1 has no correct example: all four models score 0/100 under strict matching. The two failure modes shown below are representative. The first, on gpt-5 (no thinking), produces a plausible-looking five-letter alphabetical string that is not in fact the DT code for the input:

<b>C1_0000</b> ground truth bcda model: abcde WRONG (typical content failure) <i>Based on the diagram, I count five crossings and compute the alphabetical DT code accordingly.</i> ANSWER: abcde
---

The second, on gpt-5 (no thinking), is a refusal that the strict scorer counts as wrong but that arguably represents a different failure mode from a content miss:

<b>C1_0009</b> ground truth bcda model: “unknown” WRONG (refusal) <i>I’m sorry, but I can’t determine a valid alphabetical DT code from this image alone. The diagram lacks the necessary over/under crossing information and consistent orientation needed to compute the DT code. If you can provide a version with clearly marked over/under crossings (or a planar diagram code), I can derive the DT string.</i> ANSWER: unknown
---

A natural follow-up question is whether the refusal reflects a more honest model: the model declines to guess when it cannot recover the over/under information. We do not score refusals separately in the canonical metric; the released JSONL files preserve the full response text so future analyses can re-score the task under a refusal-aware metric.

**D0** — does this PD code describe this image? On D0, claude-opus-4-7+thinking solves the negative-class item D0\_0100 by spotting that the PD code’s self-loop crossing has no visual counterpart in the image:

<b>D0_0100</b> <b>ground truth “no”</b> <b>model: “no”</b> <b>CORRECT</b> <i>Looking at the PD code, the crossing [12, 12, 13, 11] is a self-loop (Reidemeister-I kink), where edge 12 connects to itself at the same crossing. The image shows interlocking rectangular strands with no visible small loop / kink characteristic of an R1 self-crossing.</i> <i>ANSWER: no</i>
---

On a positive-class item, the same model defaults to “no” after an inconclusive count:

<b>D0_0083</b> <b>ground truth “yes”</b> <b>model: “no”</b> <b>WRONG (yes-class default-to-no)</b> <i>Looking at the image, I need to count the crossings and verify the structure matches the PD code with 17 crossings. The image appears to show a complex knot with multiple overlapping rectangular loops. Counting the crossings carefully in the diagram, the structure doesn't appear to match a 17-crossing configuration with the given connectivity.</i> <i>ANSWER: no</i>
---

The pair is the running shape of the D0 failure profile: negatives are answered by spotting a mismatch the model can see, and positives are answered by defaulting to “no” when the count and the connectivity cannot be verified jointly.

**A3\_I — same canonical PD, given same bucket.** A3\_I responses on the canonical run are almost always one-token (**ANSWER: yes** or **ANSWER: no**); the model does not emit a reasoning trace by default. The qualitative read is at the aggregate level: Claude scores 90.5% on this task, GPT-5 scores 63%, and turning thinking on lifts GPT-5 to 74.5% but does not move Claude. One correct and one wrong example are shown below, each on **gpt-5** without thinking. The wrong example flips the answer on what should be a positive item, presumably because the visual relabelling is not preserved across the encoder’s patches.

<b>A3_I_0001</b> <b>ground truth “yes”</b> <b>model: “yes”</b> <b>CORRECT</b> <i>ANSWER: yes</i>
---

<b>A3_I_0000</b> <b>ground truth “yes”</b> <b>model: “no”</b> <b>WRONG (positive-class flip)</b> <i>ANSWER: no</i>
---

The terse-answer pattern on A3\_I is itself a finding: the non-thinking GPT-5 does not believe the task warrants a reasoning trace, and it answers from whatever visual prior the encoder delivers. The two Claude variants reach 90.5% on the same no-reasoning-trace responses, so the gap is at the perception layer rather than at the reasoning layer.

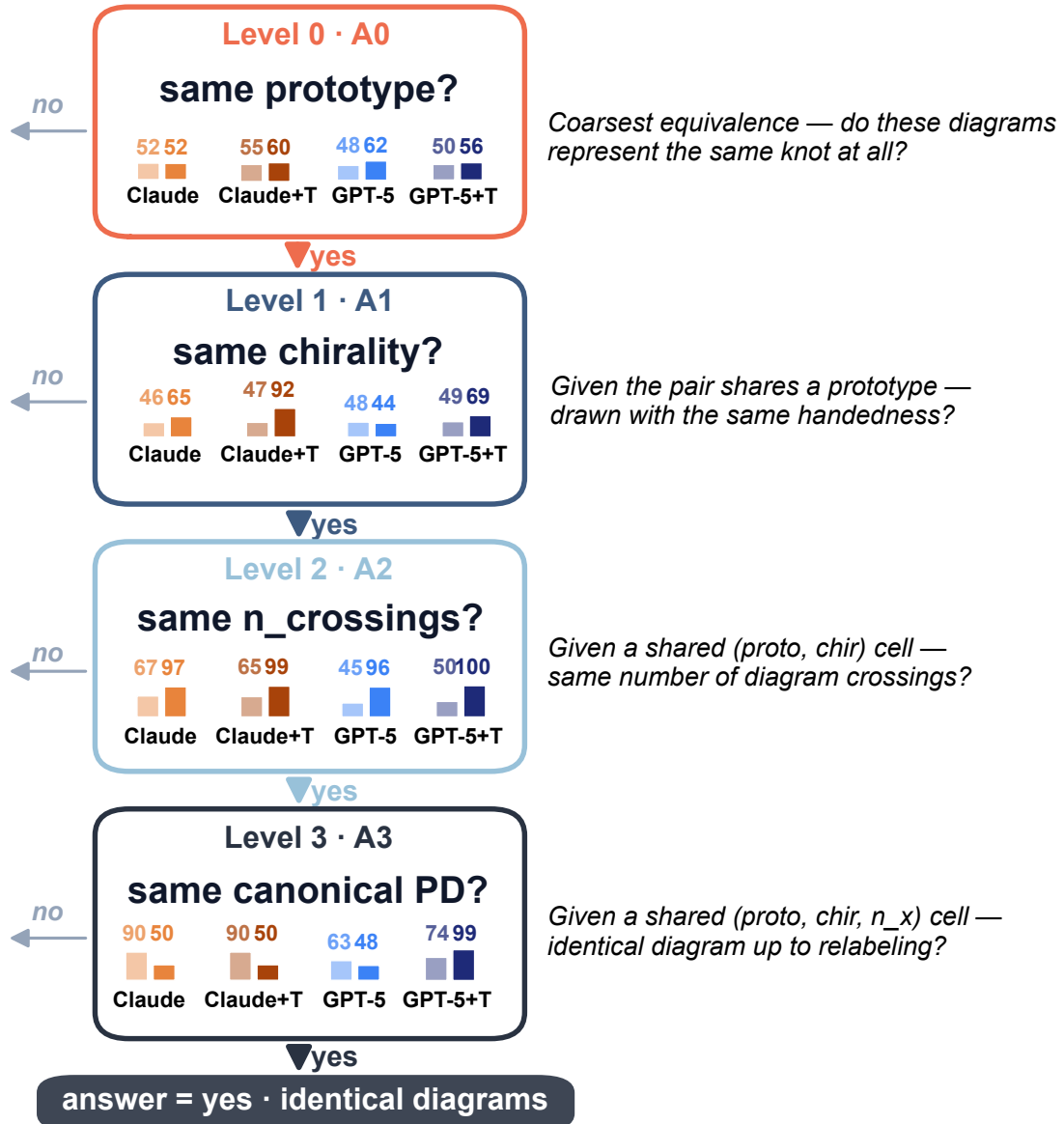


**Figure 5:** Task taxonomy. Four families decompose the operation side of the perception–operation gap: equivalence recognition (A), action prediction on a Reidemeister trajectory (B), identification (C), and cross-modal grounding (D). The -I/-S split (where applicable) controls whether the structure is delivered via pixels or via PD-code text.

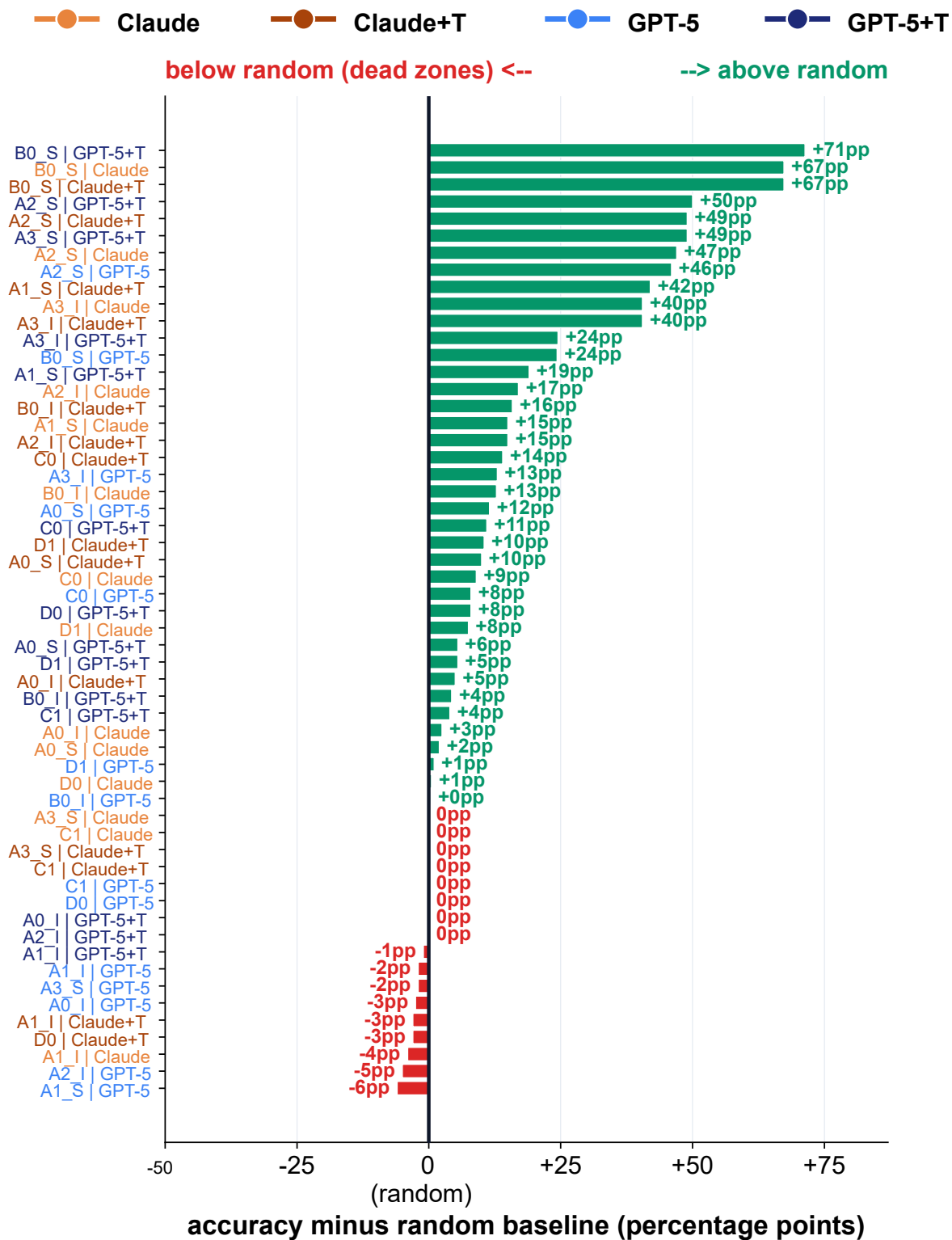


**Figure 6:** Deviation from random baseline for every (task, model) pair. Bars are color-coded by model. A bar to the right indicates better than random; to the left indicates at or below random. 15 of 56 pairs sit at or below their random baseline.

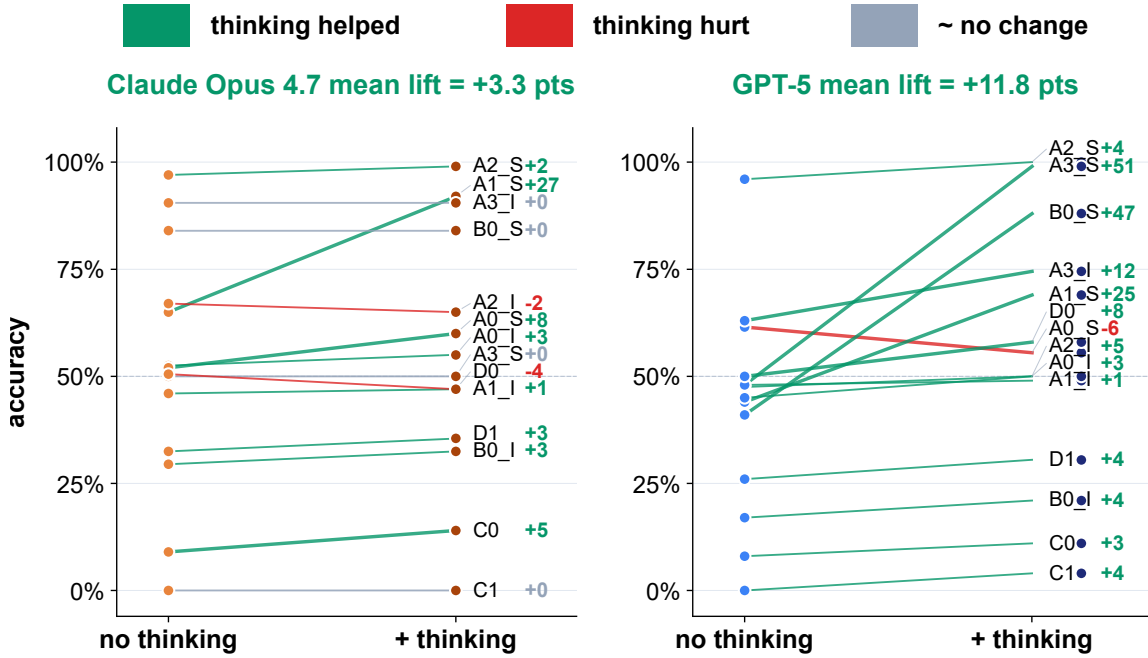


**Figure 7:** Per-task reasoning lift (no-thinking  $\rightarrow$  thinking) for each vendor. Both vendors gain from thinking; the lift concentrates on  $-S$  tasks. Image-only tasks move by single digits or fall.

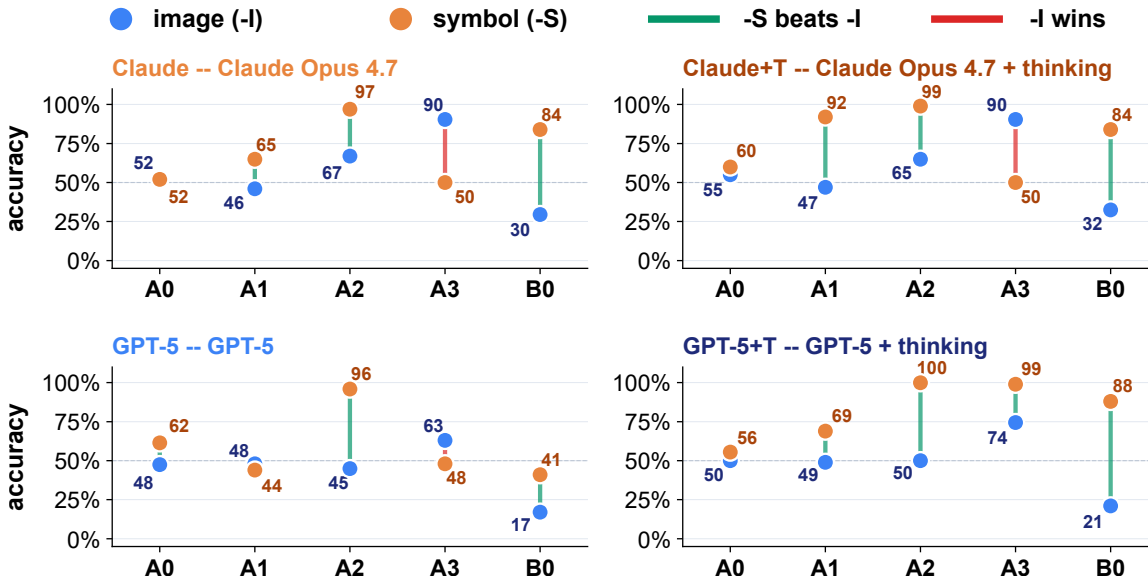


**Figure 8:** Image ( $-I$ ) vs. symbol ( $-S$ ) accuracy paired-dot scatter, one panel per model, across the families that have both modalities. Lines connect each task's two variants; green = symbol higher, red = image higher.

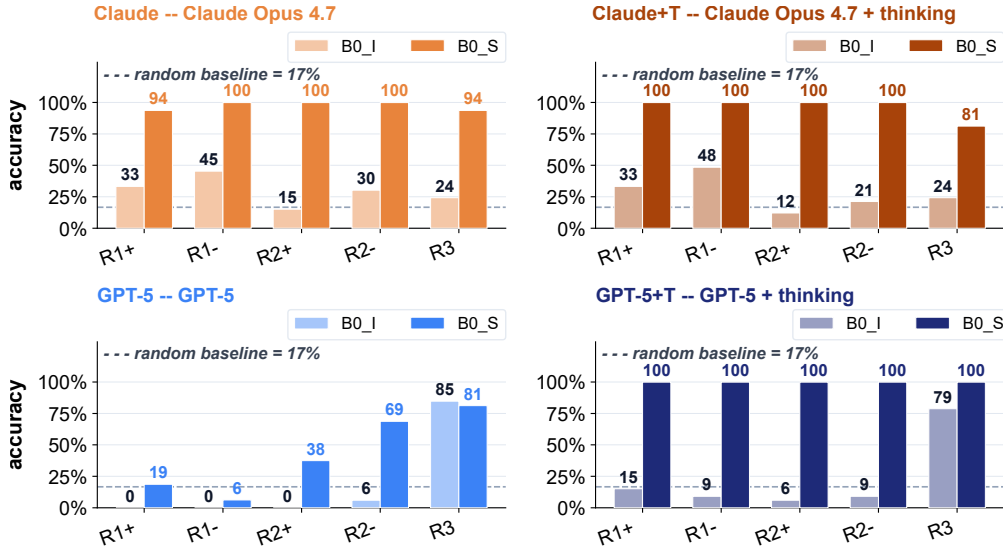


**Figure 9:** B0 per-R-move accuracy. The non-thinking GPT-5 row scores high on R3 and low on every other class, exposing an “always-R3” shortcut that the marginal distribution of its answers also confirms. Thinking removes the shortcut on the symbolic variant (B0-S) but not on the image variant (B0-I), where all four models stay below 35%.

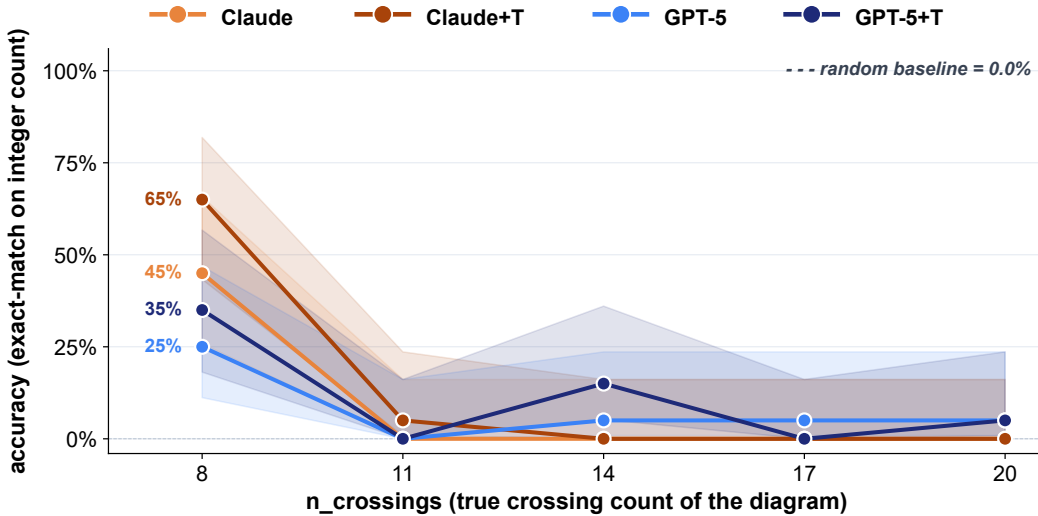


**Figure 10:** C0 crossing-count accuracy as a function of the ground-truth crossing count  $n_x$ , with Wilson 95% confidence intervals. All four models score above 50% near  $n_x = 8$ , decline sharply through  $n_x \in [10, 14]$ , and approach the chance level by  $n_x = 17$ . Strict integer match is unforgiving of  $\pm 1$  miscounts.

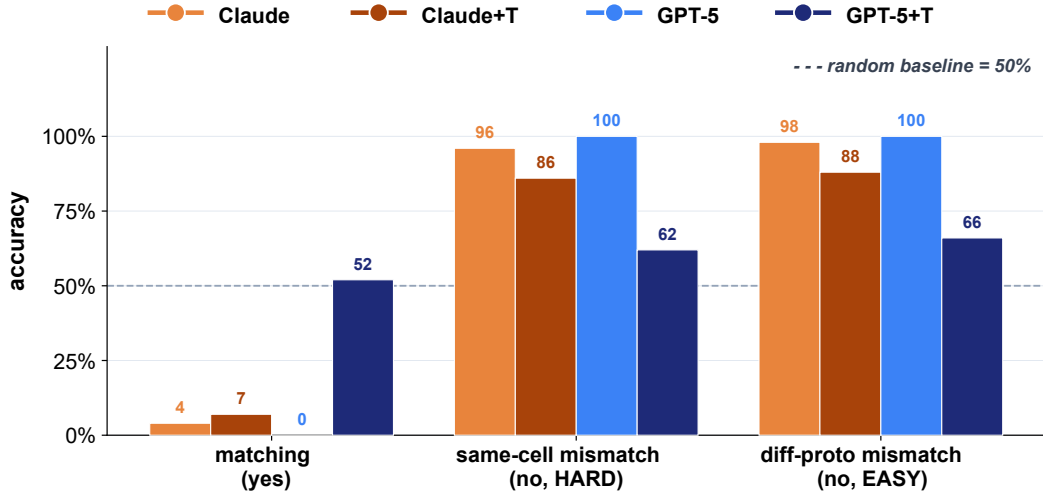


**Figure 11:** D0 per-subtype breakdown. All four models default toward “no” answers: matching items receive 0–16% “yes” answers and same-task mismatches receive 86–100% “no” answers. The asymmetry is consistent across vendors and across thinking modes.

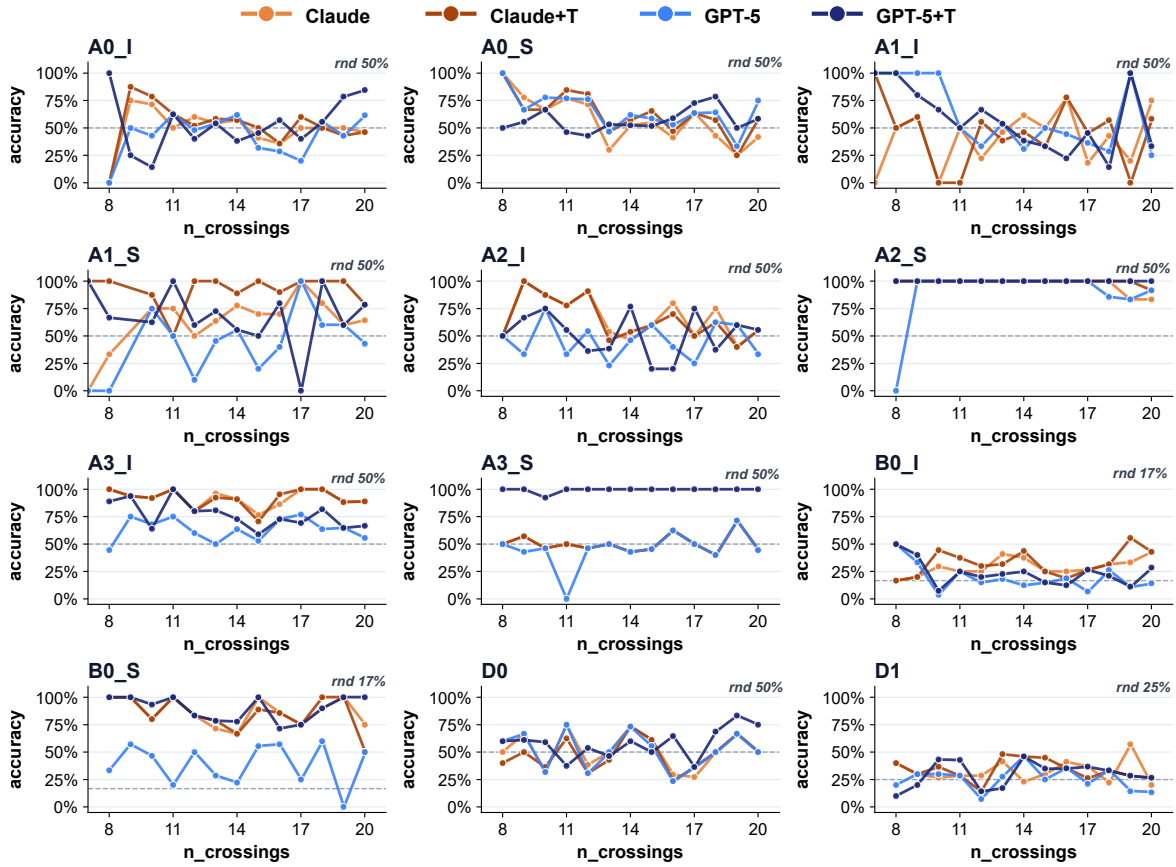


**Figure 12:** Per-task accuracy as a function of crossing count  $n_x$ , plotted per task with one panel per task and four lines per panel (one per model). The shaded band marks Wilson 95% confidence at each  $n_x$  bin.

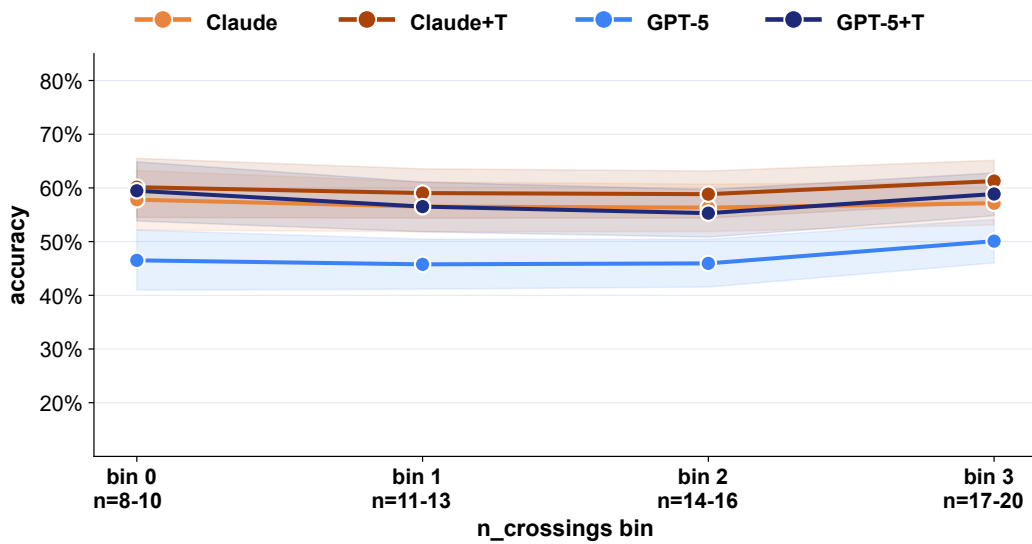


**Figure 13:** Coarse four-bin  $n_x$  gradient (8–10, 11–13, 14–16, 17–20). Tasks whose accuracy falls monotonically across the bins are the tasks where complexity is the binding constraint. Tasks that are flat-near-random across bins are bottlenecked by the operation, not by complexity.

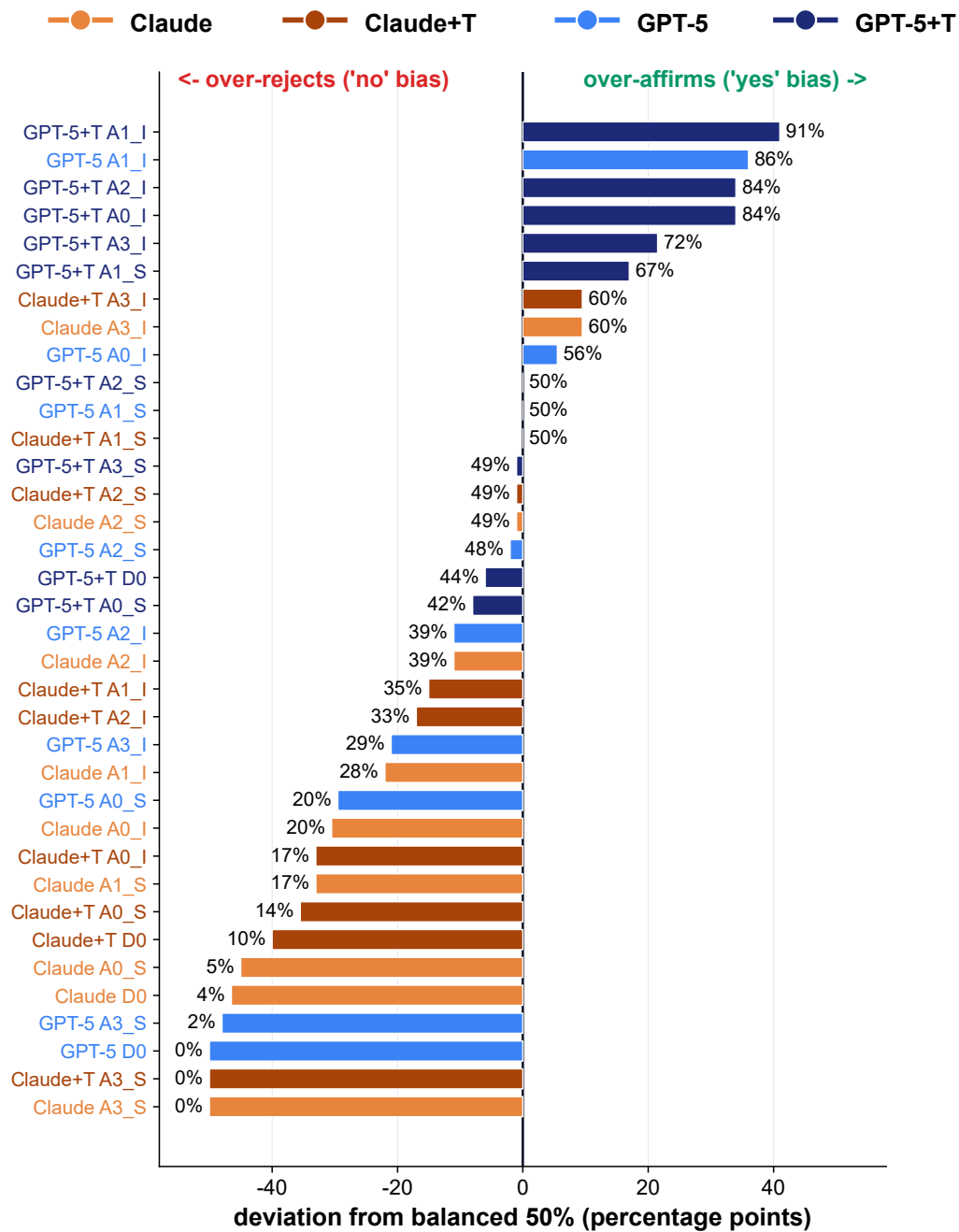


**Figure 14:** Yes-bias per binary task, per model. The bar height is the empirical rate of “yes” answers; the dashed horizontal line is the ground-truth “yes” rate for that task. D0 has the strongest no-bias of any binary task; A1\_S and A3\_S show the largest thinking-mode-induced rebalance.

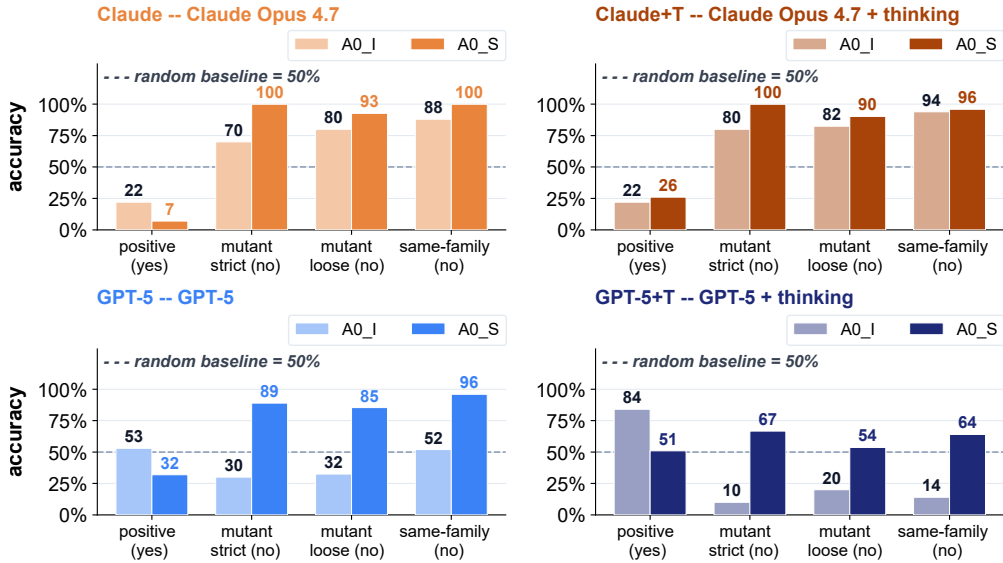


**Figure 15:** A0 accuracy on mutant negatives. The 39 strict mutant pairs (all four classical invariants collide) and 75 loose mutant pairs (Jones-only collisions) are the hardest negatives in A0. All four models score below 60% on every subtype; mutant negatives are the failure-mode that classical-invariant-only graders would miss.

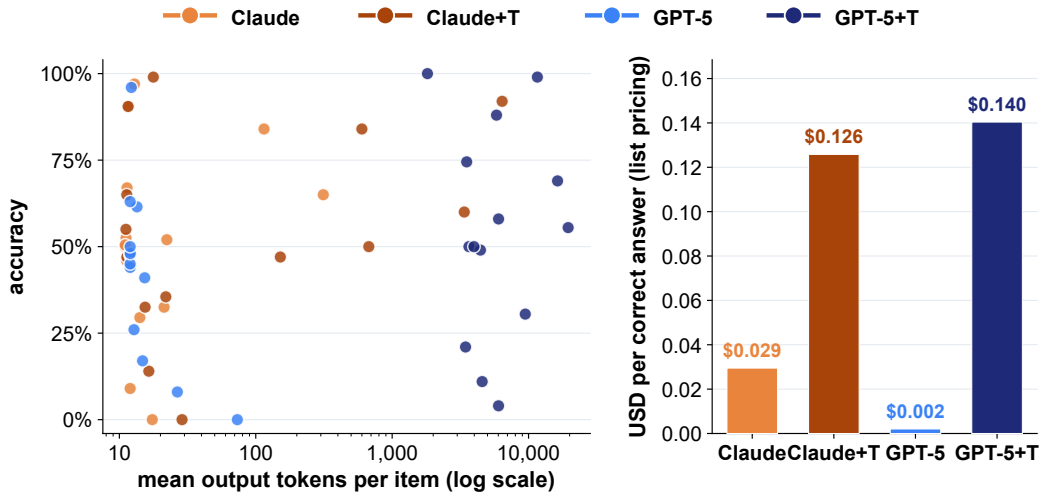


**Figure 16:** Output-token and cost summary across the four models on the canonical post-rerun. Thinking modes are 6–8× the output-token volume of their non-thinking counterparts; cost scales linearly with output tokens at the published per-token rates.

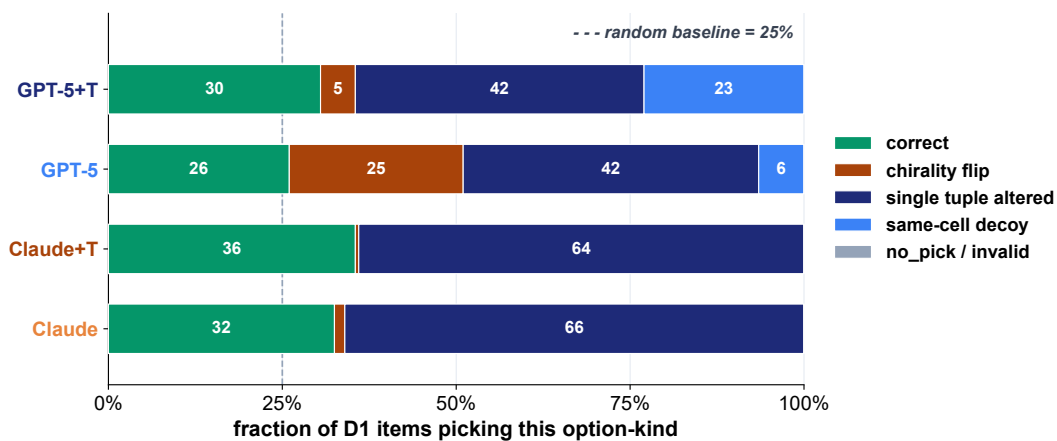


**Figure 17:** D1 confusion over the four-letter option set. The distribution of model-emitted letters is near-uniform for all four models; even when the model is correct, the letter choice is rarely content-driven.

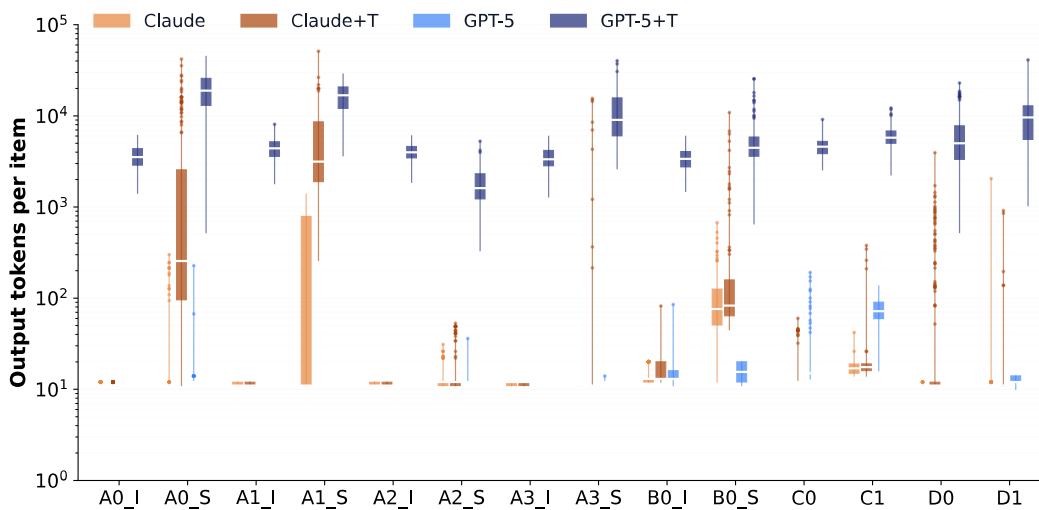


**Figure 18:** Output-token distribution per task, per model. The long tails on the thinking-mode rows correspond to runs that nearly exhaust the 64K extended-thinking budget; the 23 empty responses across the four models live in those tails.